JOURNAL OF GEOPHYSICAL RESEARCH: SOLID EARTH, VOL. 118, 4378–4397, doi:10.1002/jgrb.50258, 2013

Lithospheric structure of an Archean craton and adjacent mobile belt revealed from 2-D and 3-D inversion of magnetotelluric data: Example from southern Congo craton in northern Namibia

T. D. Khoza,[1,2] A. G. Jones,[1] M. R. Muller,[1] R. L. Evans,[3] M. P. Miensopust,[1,4] and S. J. Webb[2]

Received 14 May 2013; revised 18 June 2013; accepted 20 June 2013; published 9 August 2013.

[1] Archean cratons, and the stitching Proterozoic orogenic belts on their flanks, form an integral part of the Southern Africa tectonic landscape. Of these, virtually nothing is known of the position and thickness of the southern boundary of the composite Congo craton and the Neoproterozoic Pan-African orogenic belt due to thick sedimentary cover. We present the first lithospheric-scale geophysical study of that cryptic boundary and define its geometry at depth. Our results are derived from two-dimensional (2-D) and three-dimensional (3-D) inversion of magnetotelluric data acquired along four semiparallel profiles crossing the Kalahari craton across the Damara-Ghanzi-Chobe belts (DGC) and extending into the Congo craton. Two-dimensional and three-dimensional electrical resistivity models show significant lateral variation in the crust and upper mantle across strike from the younger DGC orogen to the older adjacent cratons. We find Damara belt lithosphere to be more conductive and significantly thinner than that of the adjacent Congo craton. The Congo craton is characterized by very thick (to depths of 250 km) and resistive (i.e., cold) lithosphere. Resistive upper crustal features are interpreted as caused by igneous intrusions emplaced during Pan-African magmatism. Graphite-bearing calcite marbles and sulfides are widespread in the Damara belt and account for the high crustal conductivity in the Central Zone. The resistivity models provide new constraints on the southern extent of the greater Congo craton and suggest that the current boundary drawn on geological maps needs revision and that the craton should be extended further south.

Citation: Khoza, T. D., A. G. Jones, M. R. Muller, R. L. Evans, M. P. Miensopust, and S. J. Webb (2013), Lithospheric structure of an Archean craton and adjacent mobile belt revealed from 2-D and 3-D inversion of magnetotelluric data: Example from southern Congo craton in northern Namibia, *J. Geophys. Res. Solid Earth*, *118*, 4378–4397, doi:10.1002/jgrb.50258.

1. Introduction

[2] The African tectonic landscape is comprised of a number of relatively stable Archean cratons that are flanked and stitched together by younger Proterozoic fold belts. The cratonic margins, and intracratonic domain boundaries, have played a major role in the Phanerozoic tectonics of southern Africa by focusing ascending magmas and localizing cycles of extension and rifting [*Begg et al.*, 2009]. The characteristic feature of cratons is their thick lithosphere, but their formation and evolution remains elusive and is the central focus of geoscientific studies. The identification of major tectonic events is complicated by lack of knowledge of lithospheric structures and their geometries beneath the surface expression of these orogens and cratons. Deep-probing magnetotelluric (MT) information is providing critical data in aiding the understanding of the formation and deformation of Pre-Cambrian orogens.

[3] In southern Africa, the greater composite Kalahari craton is separated from the composite Congo craton by the NE-SW trending Damara-Ghanzi-Chobe belts (Damara belt is in Namibia, and its extension in Botswana is called Ghanzi-Chobe), henceforth collectively called DGC (Figure 1), a component of Gondwanan Pan-African orogenic belts. Due to the huge amount of geochemical [*Griffin et al.*, 2003], seismic [*James et al.*, 2001], and electrical [*Jones et al.*, 2009; *Muller et al.*, 2009; *Evans et al.*, 2011; *Miensopust et al.*, 2011] data, a lot is known about the Kalahari craton, which includes in its core the Kaapvaal craton. What is not fully understood is the lithospheric structure and geometry of the Congo craton, north of the Kalahari

[1]School of Cosmic Physics, Dublin Institute for Advanced Studies, Dublin, Ireland.
[2]School of Geosciences, University of the Witwatersrand, Johannesburg, South Africa.
[3]Department of Geology and Geophysics, Woods Hole Oceanographic Institution, Woods Hole, Massachusetts, USA.
[4]Institut für Geophysik, Westfälische Wilhelms-Universität Münster, Münster, Germany.

Corresponding author: T. D. Khoza, Dublin Institute for Advanced Studies, School of Cosmic Physics, 5 Merrion Square, Dublin, Ireland. (davidkhoza@cp.dias.ie)

2169-9313/13/10.1002/jgrb.50258

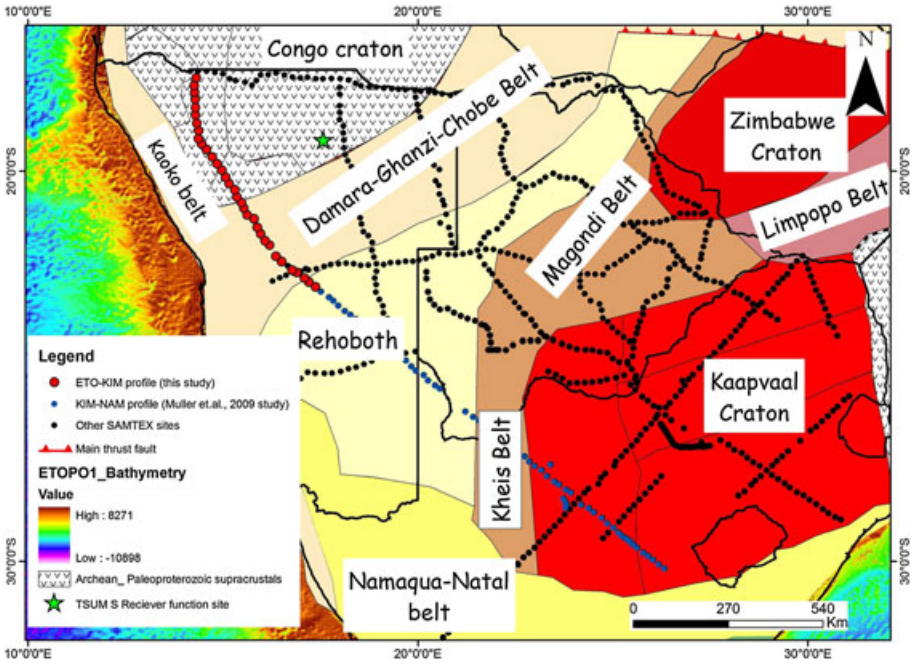

Figure 1. Main tectonic provinces making up the Southern African lithosphere (modified from *Begg et al.* [2009] and the Pre-Cambrian basement of *Singletary et al.* [2003]). The locations of the Southern African Magnetotelluric Experiment (SAMTEX) MT sites (black-filled circles) are shown with the ETO-KIM (Etosha-to-Kimberly) profile stations shown as red filled circles and the blue filled circles are the KIM-NAM (Kimberly-to-Namibia) profile published in *Muller et al.* [2009]. The blue-filled circles shows MT sites of the ETO-KIM profile which is the focus of the 2-D inversion part of this study. Also shown are the locations of the seismic station, TSUM (Tsumeb station) (green star) from the Africa Array database (www.africaarray.psu.edu), from which *S* wave receiver functions were derived by *Hansen et al.* [2009]. The backdrop image is the bathymetry ETOPO1 of *Anamte and Eakins* [2009].

craton, particularly its southern boundary with the Damara belt in north central Namibia and northwestern Botswana.

[4] The composite Congo craton comprises several Archean shields, the southern part comprising the Angolan shield, that consists of granite-gneisses and metasediments overlain by Paleoproterozoic cover [*Begg et al.*, 2009]. The highly complex Damara-Ghanzi-Chobe (DGC) belt, forming part of the Pan-African orogenic system, records the Neoproterozoic collision between the composite Congo and the Kalahari cratons during the amalgamation of Gondwana [*Daly*, 1986; *Prave*, 1996; *Hanson*, 2003; *Ritter et al.*, 2003; *Gray et al.*, 2006]. Thick Kalahari sedimentary cover makes it difficult to investigate the geometry of the southern Congo craton beneath the DGC belt with geological mapping. In this work, we use the deep-probing magnetotelluric technique to circumvent this problem.

[5] The Southern African Magnetotelluric Experiment (SAMTEX) is a multinational scientific project that is applying deep-probing MT to understand the present and past tectonic process in southern Africa through mapping of physical parameters and their geometries. Data at over 750 MT sites were collected during four phases of acquisition. In the third and fourth phases, MT data were acquired along four N-S and two E-W profiles crossing the Damara belt and the southern Congo craton (Figure 1), in addition to the other profiles that will be presented elsewhere.

[6] This paper has two parts; the first part concerns the 2-D isotropic and anisotropic inversion modeling and 3-D inversion, the second part is the interpretation of the models. The 2-D crustal and lithospheric models presented are of the westernmost N-S ETO-KIM profile, which is an extension of the KIM-NAM profile published by *Muller et al*. [2009] (see Figure 2). We chose the ETO-KIM profile for 2-D inversion as it will provide strict comparison with models from the KIM-NAM profile and provide insight into the variation in lithospheric structure/thickness from a Proterozoic terrane to an Archean craton. The 3-D inversion results are derived from applying a newly developed 3-D modular electromagnetic modeling (*ModEM*) code of *Egbert and Kelbert* [2012] on MT data from 88 stations distributed across the DGC and the southern Congo craton (see Figure 3 for site locations). The overarching objective of our study is to map the deep electrical structure of the Congo craton and its flanking Damara orogen and to understand the nature of the cryptic boundary between these two geological domains.

[7] The magnetotelluric (MT) method has been used extensively in similar Archean and Proterozoic terrains [*Jones et al*., 2002; *Wu et al*., 2005; *Jones et al*., 2005a; *Selway et al*., 2006; *Spratt et al*., 2009; *Muller et al*., 2009; *Miensopust et al*., 2011] to image the geometry of cratonic blocks and infer the tectonic histories of Pre-Cambrian collisional margins. *Muller et al.* [2009], *Evans et al.* [2011], and *Fullea et al.* [2011] showed how electrical resistivity data can be used to infer the depth to the thermal thickness of the lithosphere by comparing the results with

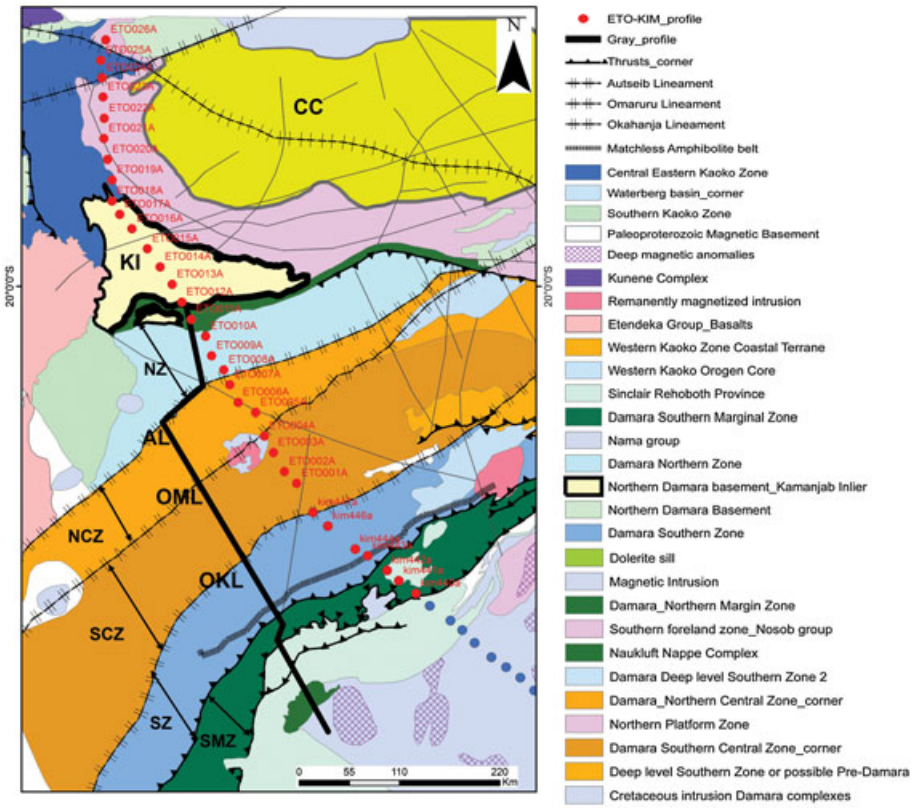

Figure 2. Detailed geology of northwestern Namibia modified from *Corner* [2008]. Deep-seated NE-SW trending faults (Okahanja and Autseb lineaments) separating various Damara belt units are mapped. The thick black line shows the profile over which the geological section in Figure 4 was generated. Also shown is the Kamanjab inlier (KI) which forms a part of the Archean basement of the Congo craton. The stratigraphic subdivisions are based on metamorphic, structural, and surface geological mapping. CC = Congo craton outline inferred by *Corner* [2008], AL = Autseib Lineament, OML = Omaruru Lineament, OKL = Okahanja Lineament.

xenolith-constrained P-T geotherms and their intersections with the mantle adiabat. Electrical resistivity of mantle rocks is primarily sensitive to temperature [*Constable et al.*, 1992; *Xu*, 2000; *Jones et al.*, 2009] and water content [e.g., *Karato*, 1990; *Jones et al.*, 2012], while crustal resistivities are a function of interconnected conductive mineral phases (e.g., sulfides, graphite, and oxides) [e.g., *Duba et al.*, 1994].

2. Geological Framework

[8] The Congo craton, which occupies a large part of central and southern Africa, comprises several Archean shields, the southwestern part of it comprising the Angolan shield that consists of granite-gneisses and metasediments overlain by Paleoproterozic cover [*Begg et al.*, 2009]. Thick Kalahari sedimentary cover leaves the southern Congo craton, and particularly its boundary with the DGC, virtually unknown and poorly understood.

[9] The Damara orogen is a three branch system reflecting part of West Gondwana suture and a collisional triple junction between the Congo and Kalahari cratons in southern Africa and Rio de Plata craton in South America [*Gray et al.*, 2008; *Frimmel*, 1998]. Two coastal branches, the Kaoko belt and Gariep belt, lie parallel to the present Namibia coast while the Damara-Ghanzi-Chobe belt (DGC) forms the NE-SW trending "Inland branch" or "intracratonic branch" [*Martin and Porada*, 1977]. The DGC, which went through a complete Wilson cycle, records the high-angle convergence of the composite Kalahari craton to the south with the composite Congo craton to the north during Pan-African amalgamation of Gondwana [*Gray et al.*, 2006]. The Braziliano orogens, Riberia, and Dom Feliciano complete the orogenic systems that define the amalgamation sutures of West Gondwana between the South American and African cratonic nuclei. The aggregation of West Gondwana involved the closing of the Adamastor Ocean between the Rio de la Plata and Kalahari cratons (forming the Kaoko and Gariep Belts) and the Khomas Ocean between the Congo and Kalahari cratons (forming the Damara Belt) [*Goscombe et al.*, 2003; *Gray et al.*, 2006]. The lack of definitive evidence of subduction-related material (i.e., ophiolite and blueschist facies metamorphism) has often being cited as evidence against Khomas ocean closure as the Kalahari craton subducted northward under the leading edge of the Congo craton. *Martin and Porada* [1977], *Porada* [1989], and *Trompette* [1997] proposed that the Damara orogenic system developed in a continental rift setting around 1000 Ma, and the DGC represents a failed rift or aulocogen that was followed by basin closure at circa 520 Ma. However, mid-ocean ridge basalt-type geochemistry in the

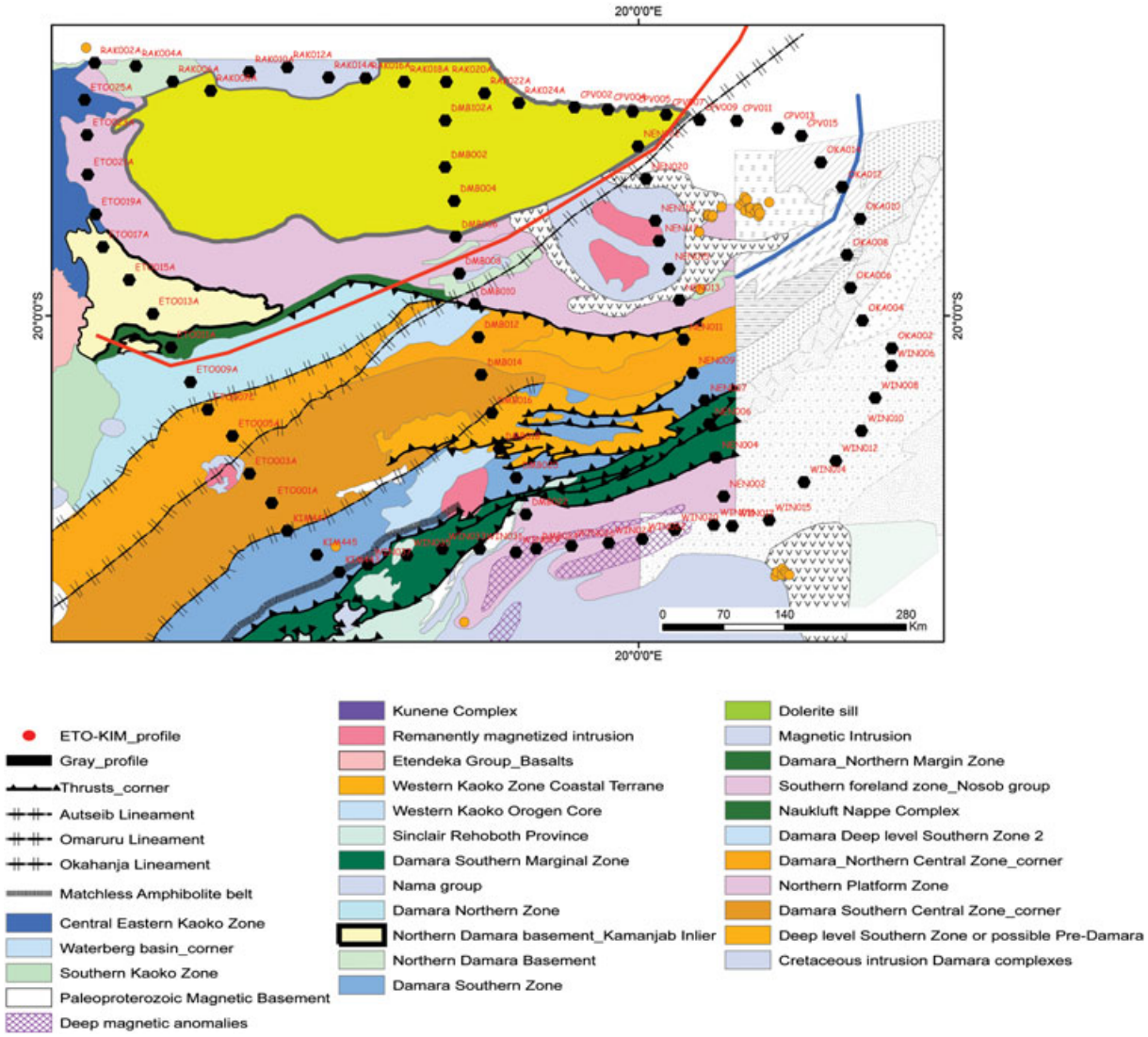

Figure 3. MT stations (black-filled circles) used for 3-D inversion, plotted on the geology map, modified from *Corner* [2008] (Namibia) and *Singletary et al.* [2003] (Botswana). Also shown are the locations of diamondiferous and no-diamondiferous kimberlites (sourced from https://consorem.uqac.ca/kimberlite/kimberlites.html). The green-filled circle shows the location of the Africa Array TSUM seismic station from which *S* wave receiver function were derived [*Hansen et al.*, 2009]. The outline of the Congo craton defined by *Begg et al.* [2009] (thick red line) and *Singletary et al.* [2003] (thick blue line) are shown.

intensely deformed pillow basalts, chert, and gabbros of the Matchless Amphibolite Belt in the DGC Southern Zone and the reported eclogites in the Zambezi Belt, which forms a continuation of the Damara belt in Zambia [*Gray et al.*, 2008; *Barnes and Sawyer*, 1980], are increasingly providing support for the subduction hypothesis.

[10] The major geological units of the Damara belt (Figures 2 and 3) include passive margin carbonate sequences and basal rift-related and deep turbiditic sediments deposited in the period spanning the Neoproterozoic time from 770 to 600 Ma [*Miller*, 1983; *Hoffmann*, 1994; *Prave*, 1996; *Frimmel*, 1998; *Goscombe*, 2004]. The collision of the Kalahari and Congo cratons terminated the deposition of the marine sedimentary sequence in Neoproterozoic time, with peak metamorphism as a consequence of collision occurring in the Middle Cambrian to Lower Ordovician periods between 534 Ma and 508 Ma [*Miller*, 1983; *Raab*, 2002]. The sequence was intruded by granotoid material during Pan-African Damara orogeny in late Neoprotorozoic-Cambrian times. Contrasting metamorphic (i.e., high temperatures/low temperatures in the center and margins of the orogen, respectively) and structural deformation patterns associated with the collision of the Kalahari and Congo cratons are observed across strike of the DGC crust. Pre-Damara basement is exposed as large Archaean-Proterozoic age inliers (Kamanjab and Kunene complex) in northern Namibia. The sedimentary sequences were deposited on top of these basement granotoids/gneisses, preserved partly as the leading edge of the Congo craton [*Gray et al.*, 2008]. The envisaged crustal geometry is

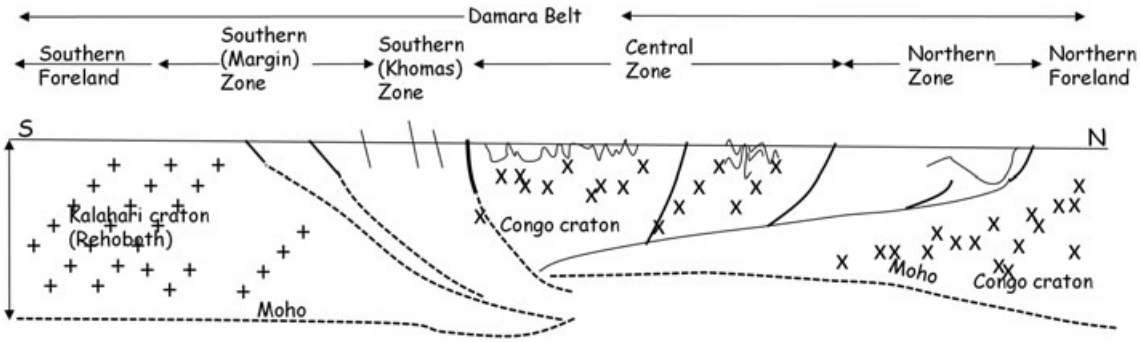

Figure 4. Cross-sectional profile showing the simplified crustal architecture of the Inland Branch of the Damara Orogen (modified from *Miller* [1988] and *Gray et al.* [2006]. See Figure 2 for location of the profile (thick black line)). The Moho depth was estimated from off-shore seismic information [*Fernàndez et al.*, 2010], and recent *S* wave receiver function results [*Hansen et al.*, 2009] from the TSUM station shown in Figure 1.

shown in Figure 4, and the tectonostratigraphic subdivisions with the DGC are based on the metamorphic, structural, and geological mapping. Moho depth is interpolated from off-shore seismics, and *S* wave receiver functions at a few locations (see location of SRF site by *Hansen et al.* [2009] in Figure 3).

[11] Like the Congo craton, the Kalahari craton is a composite craton composed of several Archean and Proterozoic blocks. Herein, we follow the *Jacobs et al.* [2008] definition of the Kalahari craton, which includes the Archean Kaapvaal and Zimbabwe cratons, separated by the high-grade metamorphic Limpopo belt, in addition to Paleoproterozoic components (Rehoboth, Okwa, and Magondi terranes). The Kalahari craton acted as a stable cratonic block with respect to the later tectonics of the Namaqua-Natal mobile belt and the Pan-African orogeny that defined the final stages of the development of the DGC. Protracted postcollision tectonothermal events within the DGC included inter alia, episodic granite emplacements, metamorphism, and structural deformation [*Gray et al.*, 2006]. The DGC belt is

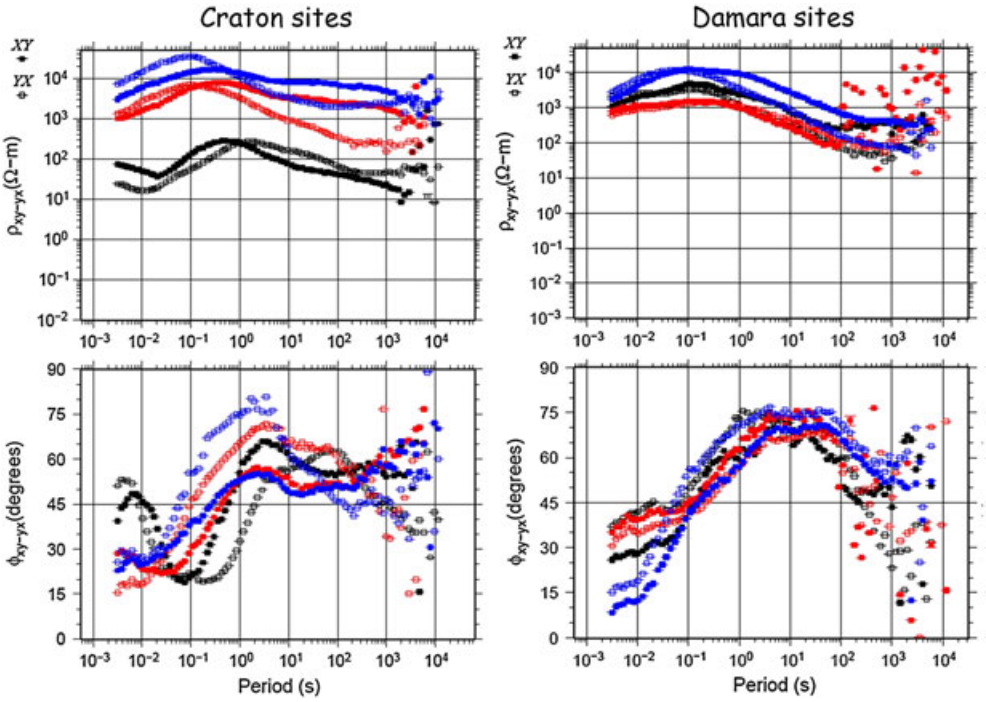

Figure 5. Examples of magnetotelluric responses from six sites: three sites on the Congo craton and three sites from the Damara orogen (color-coded). Apparent resistivity and phase responses are plotted a function of increasing period (period being proxy for increasing depth). Both the transverse electric (*XY*) mode (currents flowing parallel to strike) and transverse magnetic (*YX*) mode (currents crossing strike) are shown. The data at most stations were generally good up to 8000 s.

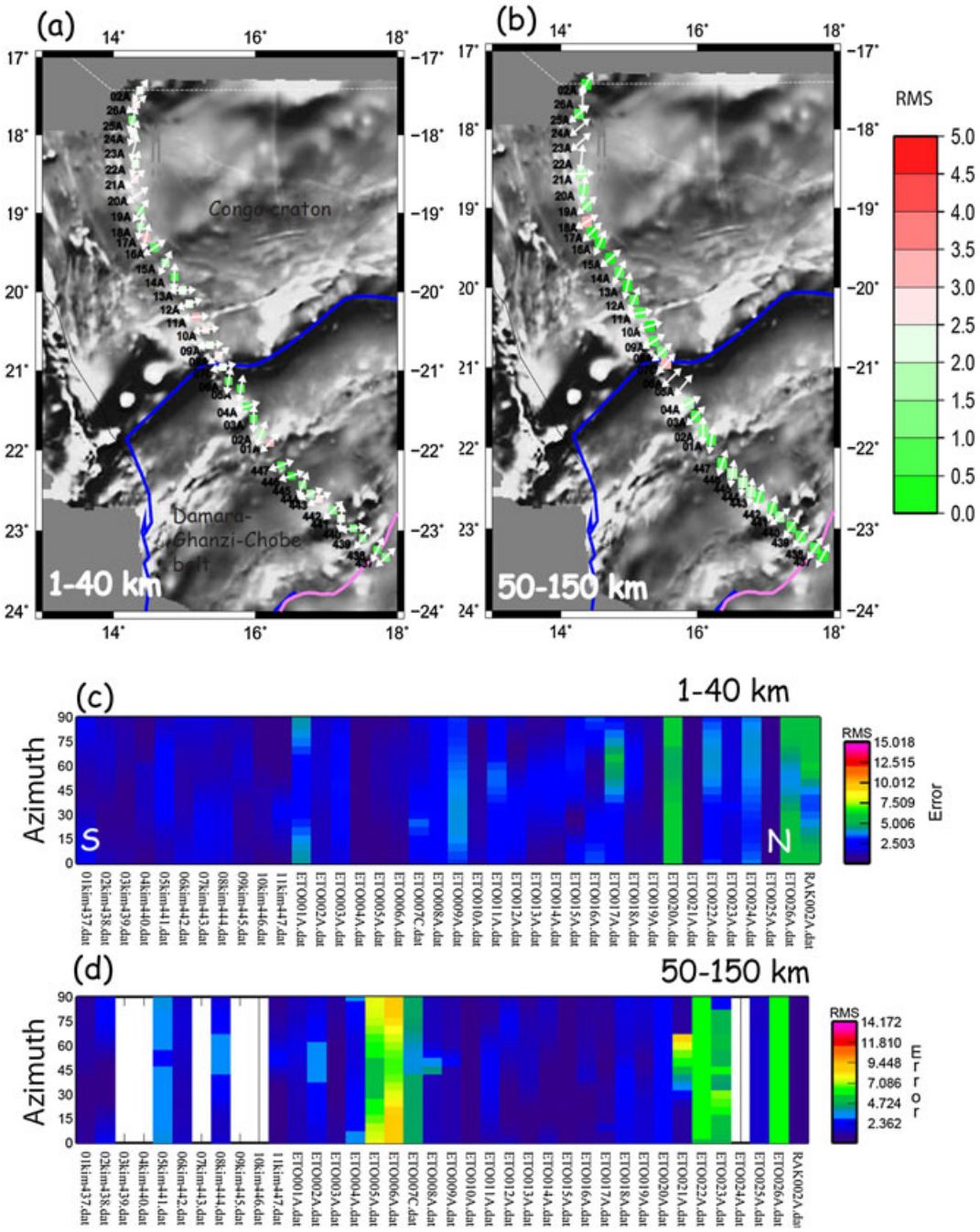

Figure 6. Results of MT data decomposition for (a) crustal (1–40 km) and (b) mantle depths (50–150 km) using *Groom and Bailey* [1989] and *McNeice and Jones* [2001] superimposed on the regional magnetic map of southern Africa. Note that there is a 90° ambiguity in the determination of the geoelectric strike: the directions shown (white vectors) have been plotted in the quadrant containing the dominant geologic strike direction observed at the surface, i.e., in the range 0° and 90°E of N. At most sites, the subsurface electrical structure is 1-D/2-D and in a few sites weakly 3-D. Sensitivity to strike direction for (c) crust and (d) mantle depths shows that only a few sites are strongly sensitive to strike direction, where low RMS values (<2) are defined over a limited range of azimuths. Other sites are relatively insensitive to strike direction and are characterized by low RMS values.

overlain by thick Cenozoic Kalahari sediments, particularly in northwestern Botswana, and airborne magnetic and gravity patterns have been used as tools to map its spatial extent.

3. Previous Geophysical Studies

[12] Previous electrical and electromagnetic studies of the DGC include the late 1970s and early 1980s magnetovariational and Schlumberger soundings by *de Beer et al.* [1975,

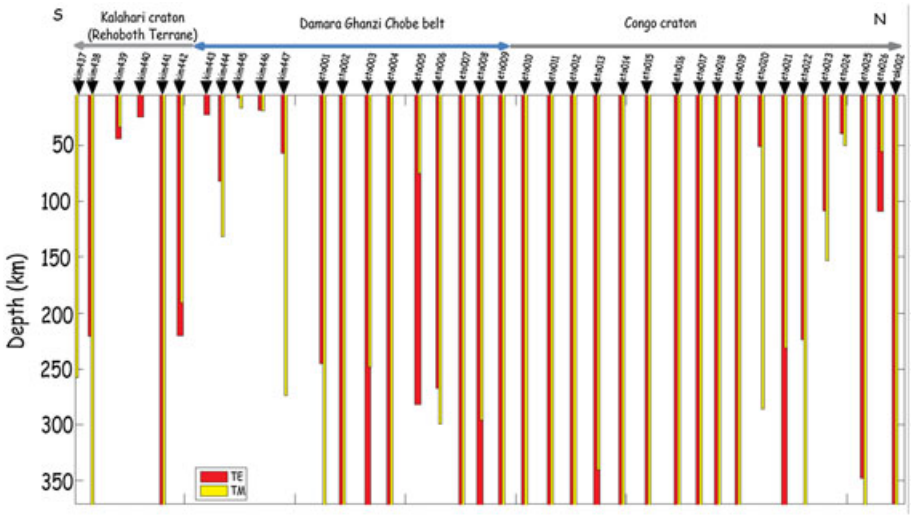

Figure 7. Niblet-Bostick depth estimates for MT stations along the ETO-KIM profile for both the TE (red bars) and TM (yellow bars) modes. While this is based on 1-D approximations, it gives in indication as to the depth sensitivity of the MT response for each site.

1976, 1982] and *van Zijl and de Beer* [1983]. These studies were the first to discover the along-strike crustal conductor within the DGC that extends from Namibia into Botswana. Serpentinized lower crust was, at the time, thought to be the cause of the elevated conductivity.

[13] In 1998 and 1999, the GeoForschungsZentrum conducted a crustal-scale study along a 200 km-long profile with a site spacing of 4 to 12 km and a focused 3-D array of 60 sites with a site spacing of 500 m to 2 km across the Waterberg Fault-Omaruru Lineament [*Ritter et al.*, 2003]. In addition to mapping the middle to lower crustal DGC conductor, *Ritter et al.* [2003] imaged a very resistive upper crust (granites) and two subvertical conductors, the Autseib and Omaruru Lineaments. The authors invoke graphite concentration to explain the conductivity along upper crustal lineaments and middle to lower crustal anomaly, the latter being along shear deep-seated shear planes. In a related study, *Weckmann* [2003] used MT phases to reveal a conductive ring structure in the shallow crust, with crustal-scale electrical anisotropy and an elongated conductor running subparallel to the Waterberg Fault-Omaruru Lineament.

[14] *Muller et al.* [2009] presented a lithospheric-scale resistivity study of the Rehoboth terrane, partially extending into the DGC belt, which showed significant lithospheric thickness, electrical, and thermal variations from older to younger terranes. *Muller et al.* [2009] found the lithospheric thickness of the DGC to be approximately 160 km. Further east on the eastern border of Botswana, *Miensopust et al*. [2011] mapped the Ghanzi-Chobe belt having resistive 180 km thick lithospheric mantle.

4. Magnetotelluric Method

[15] Magnetotellurics (MT) is a passive-source electromagnetic sounding technique that uses the time-varying ionospheric magnetic fields as its source for periods greater than 0.1 s (i.e., deep crustal and mantle probing periods) [*Chave and Jones*, 2012]. Mathematically, MT responses are represented by a complex impedance tensor **Z** in the frequency domain (also known as the MT transfer function or MT response function), which defines the linear relation between the electric (**E**) and magnetic (**H**) field vectors. On surface, simultaneous measurements of the three magnetic field components (H_x, H_y, and H_z) and the two horizontal electric fields (E_x and E_y) are recorded, processed, and modeled to obtain the subsurface resistivity structure of the Earth. The ratios of the electric and magnetic fields as a function of period (which, for an electromagnetic (EM) method, is a proxy for depth) gives the lateral and depth distribution of electrical resistivity [e.g., *Jones*, 1999; *Chave and Jones*, 2012]. For the ideal 2-D Earth case, two independent modes of electric field propagation can be defined: (1) the *transverse electric* (TE) mode describes currents flowing parallel to the strike direction, and (2) the *transverse magnetic* (TM) mode which describes currents flowing perpendicular to strike direction [*Chave and Jones*, 2012].

[16] The electrical resistivity of Earth materials varies by over several orders of magnitude, which makes the MT method a superior technique for investigating geological and structural changes in the crust and mantle of physical properties. In the crust, conducting mineral phases, like graphite and sulfides, produce conductivity anomalies. In active tectonic regions (e.g., Himalayas), partial melt is thought to be responsible for observed elevated conductivities [*Unsworth et al.*, 2004; *Le Pape et al.*, 2012]. In the mantle, electrical resistivity of mantle minerals (olivine, orthopyroxene, and clinopyroxene) is primarily controlled by temperature [*Constable et al.*, 1992; *Xu*, 2000] and, to a lesser extent, compositional variations [*Jones et al.*, 2009]. In addition, dissolved hydrogen has been found to increase the conductivity of olivine in the mantle [*Karato*, 1990] although the effect on conductivity is hotly debated [*Karato*, 1990; *Yoshino et al.*, 2006; *Jones et al.*, 2009; *Karato*, 2010; *Jones et al.*, 2012]. Thus, resistivity models of the Earth provide directly the present geometrical arrangement of tectonic margins and the definition of the base of the lithosphere. Used in conjunction with geochemical and seismological information, it is possible to confidently derive the thermal

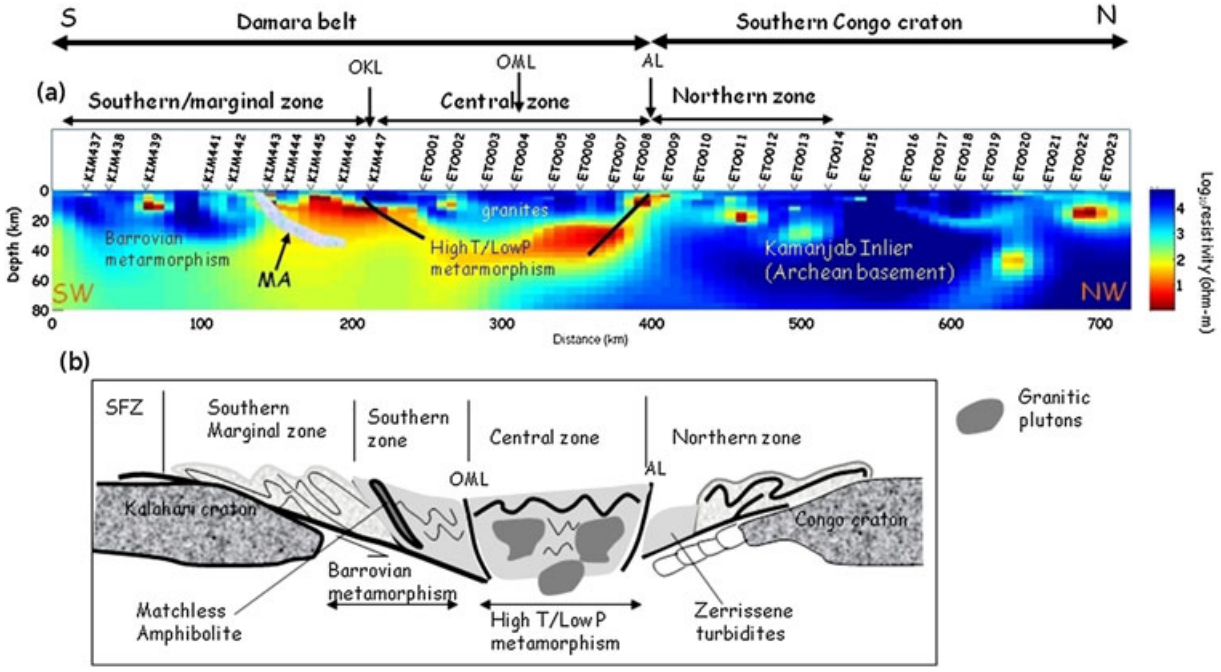

Figure 8. (a) Crustal-scale resistivity model of the ETO-KIM profile, showing the main features resolved by the inversion process. The mid-lower crustal conductors, upper crustal Pan-African granites, and the Archean basement (Kamanjab Inlier) are the major features of this model. (b) For comparison, the geological section, modified from *Gray et al.* [2007], is included. AL: Autseib Lineament, OML: Omaruru Lineament, OKL: Okahanja Lineament, MA: Matchless Amphibolite, SFZ: Southern Foreland Zone.

evolution of Pre-Cambrian regions [*Davis*, 2003; *Muller et al*., 2009; *Fullea et al*., 2011].

4.1. Data Collection and Processing

[17] The SAMTEX database comprises 750 MT stations distributed across three southern African countries: Botswana, Namibia, and South Africa (see Figure 1). During the third phase of SAMTEX, high-quality data were acquired along the N-S oriented subparallel profiles, herein referred to as *DMB* (Damara), *NEN* (Nyae-Nyae), and *OKA-WIN* (Okavango-to-Windhoek) (see Figures 2 and 3 for their location). The ETO-KIM profile (red circles in Figure 1) is the extension of the prior KIM-NAM profile (blue circles) published by *Muller et al.* [2009]; the objective of the latter was to determine the lithospheric structure and evolution of the Rehoboth Terrane and its relationship to the Kaapvaal craton. The NW-SE ETO-KIM profile and the northernmost E-W *RAK* (Ruacana-to-Katima) profile were both collected in the fourth phase. All profiles were designed to traverse over known and enigmatic tectonic terranes, with approximately 20 km separating the stations. The layout of the sites in Namibia and Botswana have a reasonable spatial distance that makes the region suitable for 3-D inversion. At each MT site, we recorded time variations of horizontal electric and magnetic fields for approximately 3 days, resulting in high-quality broadband data at periods between 0.002 s and 10,000 s. Vertical magnetic fields (H_z) were recorded at 17 sites along the ETO-KIM profile, 6 sites along the DMB profile, 5 sites along the NEN profile, and 7 sites along the OKA-WIN profile (difficult terrane precluded H_z measurements at every site). Phoenix Geophysics' instruments, MTU-5 and MTU-5A recording units and MTC-50 induction magnetometers, were used for broadband data acquisition. We also recorded long period data (10–30,000 s) at seven sites along the ETO-KIM profile, three sites on the DMB profile, four sites on the NEN profile, and four sites on the OKA-WIN profile over 3 week periods using LEMI-417M (Long Period Electromagnetic Instrument) systems manufactured by LVIV Centre of Institute of Space Research, Ukraine (http://www.isr.lviv.ua/lemi417.htm). The broadband and long period data were merged to produce a single MT response for a particular site. Where appropriate, the longer the period of recording, the deeper we image into the Earth. However, in more conductive regions, the signal penetration is attenuated due to the shielding effect of conducting materials (see section 8).

[18] Given that sites were recorded simultaneously, we employed remote referencing methods [*Gamble et al.*, 1979] to reduce bias effects. The recorded electromagnetic time series data were processed using robust techniques of *Jones and Jodicke* [1984], method 6 in *Jones et al.* [1989], *Egbert and Booker* [1986], and the heuristic approach of *Jones et al.* [1989], as implemented in the Phoenix processing software SSMT 2000, to derive MT impedance estimates that were subsequently converted to apparent resistivities and phases.

[19] Data quality was generally good for most sites; however, where severe distortion (e.g., current channeling) effects were observed that could not be treated, those sites were not used for further modeling. Figure 5 shows an example of MT responses from four sites along the ETO-KIM profile (two sites within the Damara belt and two sites on the Congo craton). For each site, apparent resistivities and the phase lags between electric and magnetic fields

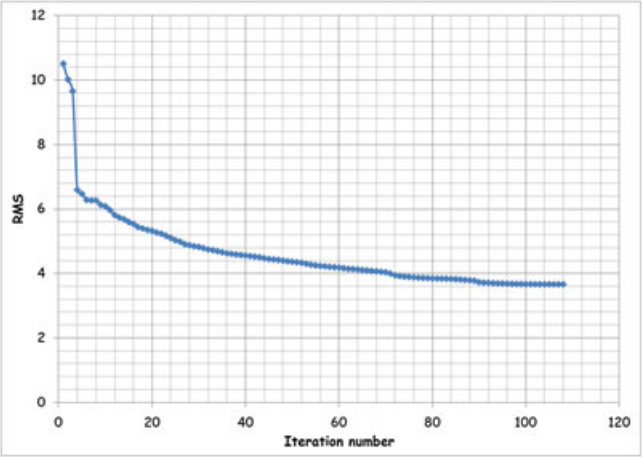

Figure 9. Variation in RMS with respect to iteration. The inversion took 69 h to complete on the STOKES cluster of the Irish Centre of High Performance Computing.

at each period are plotted against increasing period. The *Rho+* algorithm of *Parker and Booker* [1996] was used to check for internal consistency between the apparent resistivity and phase responses, including discarding spurious data points.

4.2. Data Analysis and Decomposition

[20] In MT, we collect profile (2-D) data; therefore, we approximate a 3-D Earth using 2-D techniques. Before MT data can be effectively modeled, the effects of near-surface features that distort our impedance estimates must be removed. Furthermore, the dimensionality of the data must be analyzed in order to determine the correct modeling approach, i.e., whether to adopt 1-D, 2-D, or 3-D techniques. Lastly, if the data are deemed to be 2-D, the most consistent geoelectric strike azimuth must be determined. The most widely applied dimensionality analysis tool is that of *Groom and Bailey* [1989] (later extended by *McNeice and Jones* [2001]); this is the approach we follow.

[21] Due to the large variations in the Earth's electrical conductivity, one naturally expects the depths of penetration of the EM signal to vary from site to site; so the latest version of *strike* was used that permits multisite analysis in approximate depth domain rather than by periods. Figure 6 shows the results of the single site, multiperiod decomposition determined for (a) crustal and (b) mantle depths (determined using the Niblett-Bostick transform of the determinant impedances) along both profiles. Most of the sites exhibit acceptable 2-D behavior (low RMS <2), and only a few sites exhibit residual 3-D characteristics. The sensitivity of each site to the geoelectric strike/azimuth is shown in Figure 6 for (c) crustal and (d) mantle depths. A strike direction of N50°E was found to be a reasonable average for most sites and most periods, which is consistent with the dominant tectonic fabric inferred from magnetic, structural, and geological trends. The regional MT responses for the ETO-KIM profile were therefore decomposed in the N50°E direction for further modeling using the regularized 2-D inversion package of *Rodi and Mackie* [2001] [see also *Mackie et al.*, 1993]. The depth of penetration for each MT site (Figure 7), calculated for both the TE and TM modes, was estimated using the 1-D Niblett-Bostick inversion [*Niblett and Sayn-Wittgenstein*, 1960; *Bostick Jr.*, 1977; *Jones*, 1983].

5. 2-D Inversion of MT Data

[22] In general, the resistivity of Earth's materials varies spatially in different directions, a feature termed electrical anisotropy. The cause of observed anisotropy, particularly for the mantle, is still debated, with hydrogen diffusion along olivine a-axes [*Mackwell and Kohlstedt*, 1990; *Bahr and Duba*, 2000; *Gatzemeier and Tommasi*, 2006; *Jones et al.*, 2012] and interconnectivity of a conductive mineral phase (e.g., graphite) along grain boundaries [*Jones et al.*, 1992; *Mareschal et al.*, 1995], being the primary candidates for mantle materials. The presence of anisotropy in the lithosphere is increasingly being taken into account when undertaking MT interpretation [*Baba et al*., 2006; *Martí et al*., 2010; *Evans et al*., 2011; *Miensopust et al*., 2011; *Le Pape et al*., 2012] and can manifest itself in macroscale or microscale. Crustal anisotropy can result from different orientations of fluid-filled structures (i.e., strain-induced) or layering of materials with varying physical properties [*Wannamaker*, 2005; *Miensopust and Jones*, 2011]. In the lithospheric mantle, strain-induced crystal preferred orientation (CPO) of anisotropic minerals, hydrogen diffusivity in mantle minerals, or the presence of partial melt are the known main causes for observed anisotropy [*Wannamaker*, 2005; *Yoshino et al.*, 2006]. Thus, understanding electrical anisotropy with depth has implications for the interpretational aspects of continental evolution. *Ji et al.* [1996], *Hamilton et al.* [2006], and *Eaton et al.* [2004] investigated the presence of electrical anisotropy for the Greenville Front, Kaapvaal craton, and Great Slave lake regions, respectively, in an attempt to look for a symbiotic relationship between MT and seismic anisotropy; their results varied from weak to strong correlation between observed seismic and electrical anisotropy. What is clear, however, is that tectonic processes, including those forming Neoproterozoic collisional terranes, result in observed anisotropy variations. Thus, it is important to understand anisotropy at all scales in order to infer present and past tectonic processes.

5.1. Isotropic Inversion

[23] We derived a 2-D isotropic electrical resistivity model for the ETO-KIM profile data using the finite difference code of *Rodi and Mackie* [2001]. This code uses a nonlinear conjugate gradient scheme to search for the smoothest best fit model [*Mackie and Madden*, 1993a, 1993b; *Rodi and Mackie*, 2001]. Several inversion parameters were tested in order to obtain a robust, low RMS and geologically acceptable model. The regularization parameter tau (τ) is the "smoothing" operator that controls the Tikhonov regularization trade-off between model smoothness and fitting the data. A tau value of 5 was used for the two models, after a rigorous search for the tau parameter that gives the most favorable compromise between RMS fit and model smoothness using the *L*-curve approach [*Hansen and O'Leary*, 1993]. A 100 Ωm homogeneous half-space was used as the starting model for all inversion runs. The systematic inversion approach that was followed included fitting initially the TE and TM phase responses preferentially by allocating high

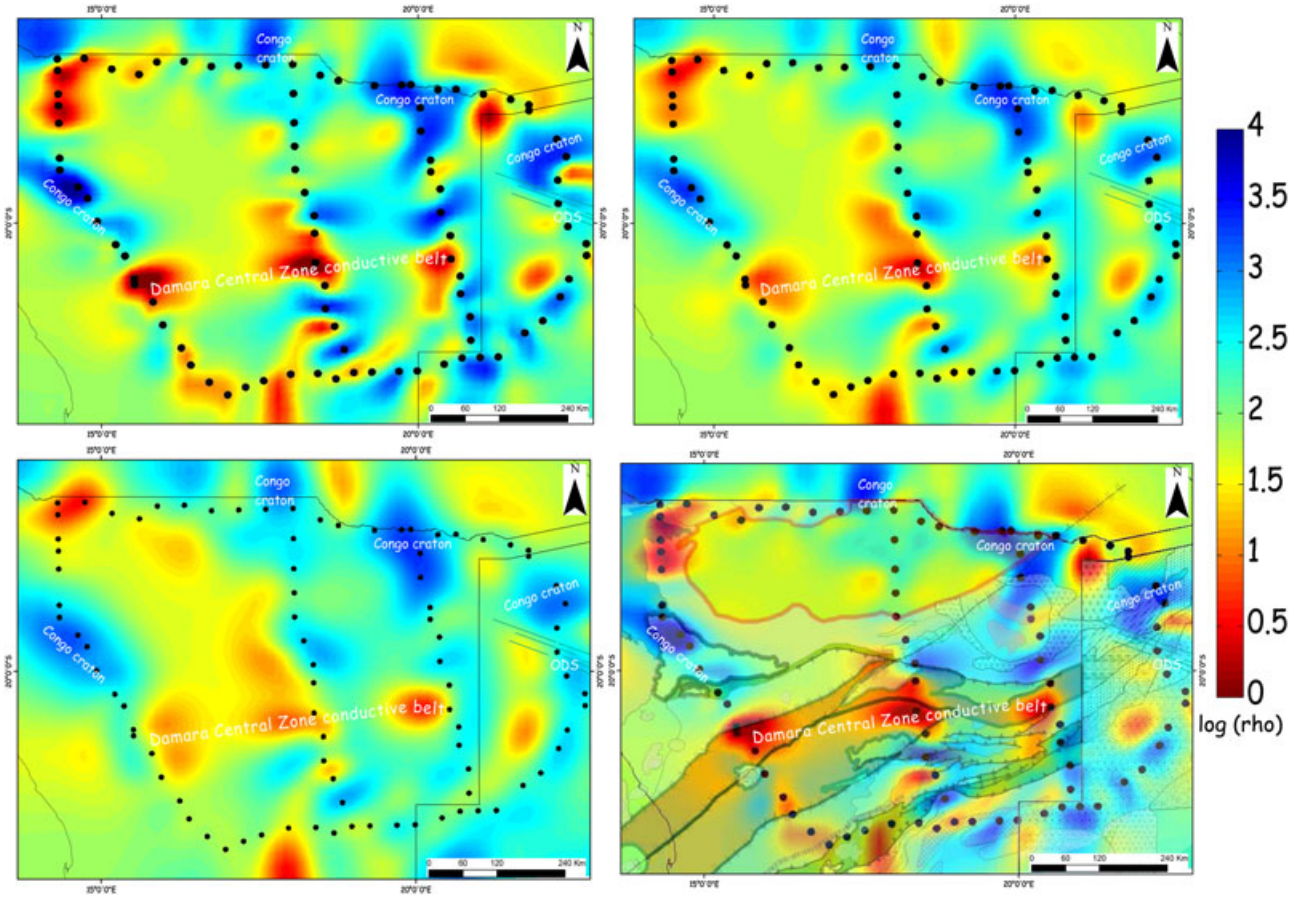

Figure 10. Resistivity maps derived from the 3-D inversion at three depths. The black-filled circles show station locations. Also shown is the 20 km resistivity slice overlain on the geology map in Figure 2. The correlation of the DGC conductor with the Central Zone is clear from this map.

error floors (50%) for the apparent resistivities. The next step was to include the apparent resistivities after some iterations by reducing the error floor, and lastly, the vertical magnetic field data were included. The reason behind inverting the phase responses first is that they are generally free of static shift effects [*Jones*, 1988]. The alpha and beta parameters in the inversion code, which control the horizontal smoothness and vertical regularization weighting, were set to 1 and 0, respectively, after testing. The final error floors were 5% for phase, 10% for apparent resistivity, and 0.02 for vertical fields. The reader is referred to *Spratt et al*. [2009] for an excellent application of the code and use of parameters. We chose to solve for the smoothest model available, since the inductive nature of the MT technique allows us to assume a smoothed structure at depth.

5.2. Anisotropic Inversion

[24] The anisotropic code we use is an extension of the isotropic code discussed above (same regularization), with an additional parameter (τ_{iso}) that controls the degree of anisotropy permitted by the inversion [*Evans et al.*, 2005; *Baba et al.*, 2006; *Evans et al.*, 2011; *Le Pape et al.*, 2012], which is how close the resistivities ρ_{xx}, ρ_{yy}, and ρ_{zz} will be to each other. A low τ_{iso} value (0) will enforce a totally anisotropic result, which means independent TE and TM mode inversions. The limitation of the code is that the anisotropic direction must coincide with the geoelectric strike direction. The resulting 2-D inversion models are shown for two different directions; one parallel (R_{xx}) and the other perpendicular (R_{yy}) to the geoelectric strike. The R_{zz} model is not shown here as it is particularly difficult to resolve due to the fact that most of the current flow in the MT problem is horizontal.

6. 3-D Inversion

[25] The inversion of magnetotelluric data in three dimensions has developed rapidly over the last couple of decades, particularly in the last few years [e.g., *Smith and Booker*, 1991; *Mackie and Madden*, 1993a; *Zhdanov et al.*, 2006; *Sasaki and Meju*, 2006; *Farquharson and Craven*, 2009; *Siripunvaraporn and Egbert*, 2009; *Egbert and Kelbert*, 2012]. The motivation for modeling the Earth in 3-D (instead of 2-D) is multifold. First, the Earth is 3-D, and it must be modeled as such for precise geological interpretation. While we collect MT data along 2-D profiles, the data we acquire and subsequently process is sensitive to 3-D conductivity variation and results in a full impedance tensor, with four complex tensor elements for each period, relating the electric and magnetic field components. Modeling all four components (Z_{xx}, Z_{xy}, Z_{yy}, and Z_{yx}) not only requires no assumptions to be made about strike directions, but

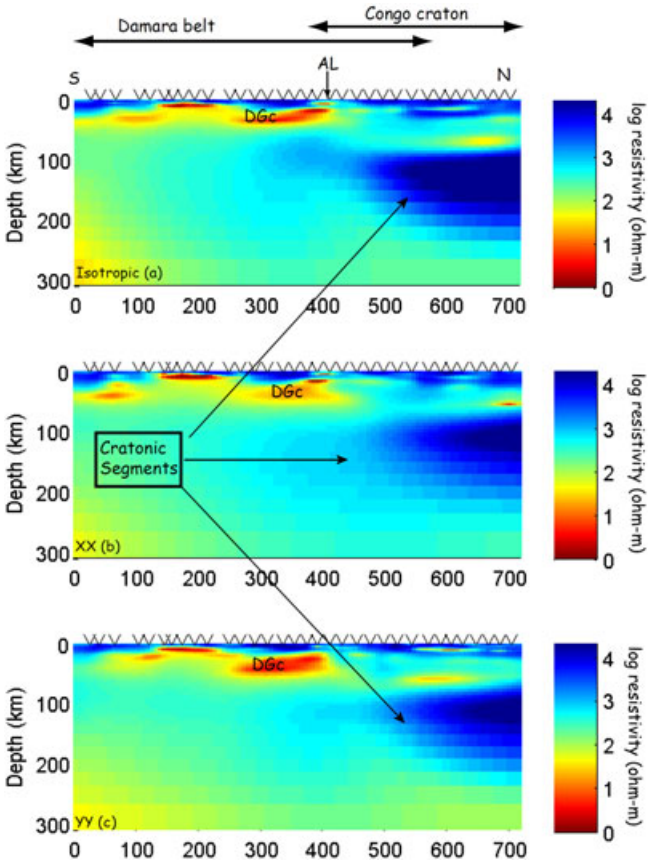

Figure 11. (a) Isotropic and (b and c) anisotropic lithospheric models of the ETO-KIM profile. Conductivity in the direction perpendicular to the profile (R_{xx}) and parallel to the profile (R_{yy}) are shown. AL: Autseib Lineament.

perhaps more importantly provides added information about the electrical resistivity structure.

[26] Second, recorded MT data often show that the validity of the 2-D assumptions fails due to the influence of 3-D subsurface structures. Depending on the inductive scale length of the target, this can lead to incorrect results if the data are modeled in 2-D. Third, the data coverage of SAMTEX stations (Figure 3) provides a reasonable spatial block that can be inverted in 3-D using a newly developed modular EM code.

[27] In this section, two different inversion schemes were applied to model our data in 3-D. We used the parallel implementation of the *WSINV3DMT* code of *Siripunvaraporn et al*. [2005], and the newly developed modular electromagnetic modeling and inversion ModEM scheme of *Egbert and Kelbert* [2012]. The WSINV3DMT is based on the 2-D data space Occam's inversion of *Siripunvaraporn and Egbert* [2000] that seeks the smoothest model to fit the data at the specified level of misfit. The ModEM inversion scheme is, as the name implies, based on a modular design where the Jacobian and sensitivity matrices are factored into several components (i.e., data functionals, forward and adjoint solvers, and model parameter mappings). The computation of the sensitivity matrix this way allows for faster computation times. Not only is ModEM suitable for large inversions (such as in our study) but also consistently resulted in models with low RMS and with geologically reasonable geometry of features. As such, we will only show the ModEM results here but the models we obtained with WSINV3DMT contained the same features. As with the 2-D models, various parameters were tested to obtain geologically plausible models. The ModEM algorithm has provision to invert up to six combinations of impedance tensor elements (Z_{xx}, Z_{xy}, Z_{yy}, and Z_{yx}) and vertical transfer functions (H_z tippers).

[28] A total of 88 stations were carefully chosen from a complete data set of 173, and inconsistent responses were edited and bad stations removed. The MT responses for each site were then decimated to 4 periods per decade with a total of 18 periods in the range 0.1–5000 s. For sites that had vertical transfer functions, a constant absolute error floor in H_z was set at 0.01.

[29] The mesh was discretized to be fairly regular in the center, with cell widths of approximately 10 km. The mesh comprised a total of 64 cells in the *X* direction, 78 cells in the *Y* direction, and 52 cells in the *Z* direction, with most stations preferentially adjusted to be located at the center of cells.

[30] Several starting models, including layered Earth models, different resistivity half-space models (100 Ωm and 200 Ωm), and various smoothing parameters (τ), were all tested and compared. A 100 Ωm prior half-space model consistently resulted in geologically consistent models with

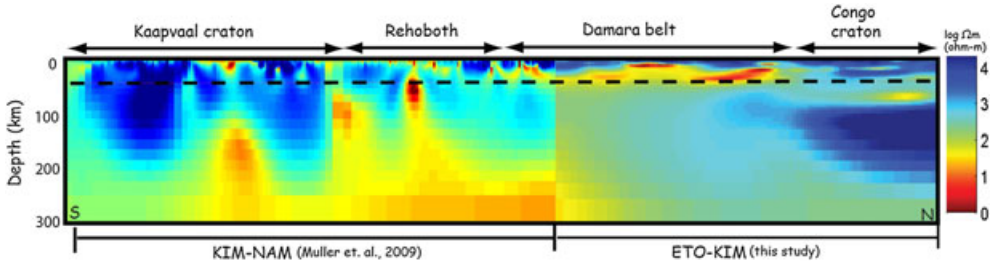

Figure 12. A model showing the combined KIM-NAM profile from *Muller et al.* [2009] and the 2-D isotropic ETO-KIM profile (see Figure 8a), depicting the current tectonic structure from the Kaapvaal craton in the SW to the Congo craton in the NW. The KIM-NAM model was derived from 2-D smooth inversion of joint apparent resistivity and phases for both TE and TM responses decomposed for 45% E of N azimuth. The algorithm used for the KIM-NAM profile was of *Rodi and Mackie* [2001] implemented in *WinGLink*®. The dotted black lines shows the approximate depth to base of lithosphere.

relatively low RMS. The final model, derived by inverting all four impedance tensor elements including the tippers, from a 100 Ωm half-space, with 10% and 15% error floors in diagonal and off-diagonal impedance elements, respectively, converged to an average RMS of 3.66 (Figures 8 and 9) after 69 h of computation using four nodes on the STOKES (SGI Altix ICE 8200EX) cluster of the Irish Centre of High Performance Computing (ICHEC, www.ichec.ie).

7. Results

7.1. Crustal Structure

[31] The 2-D inversion model (Figure 8) of the ETO-KIM profile reveals a complex crustal structure dominated by three main features that correlate relatively well with known structural and geological features: (1) the upper crustal resistive structures, (2) the middle to lower crustal conductive zone, and (3) the high resistivity Kamanjab Inlier to the north.

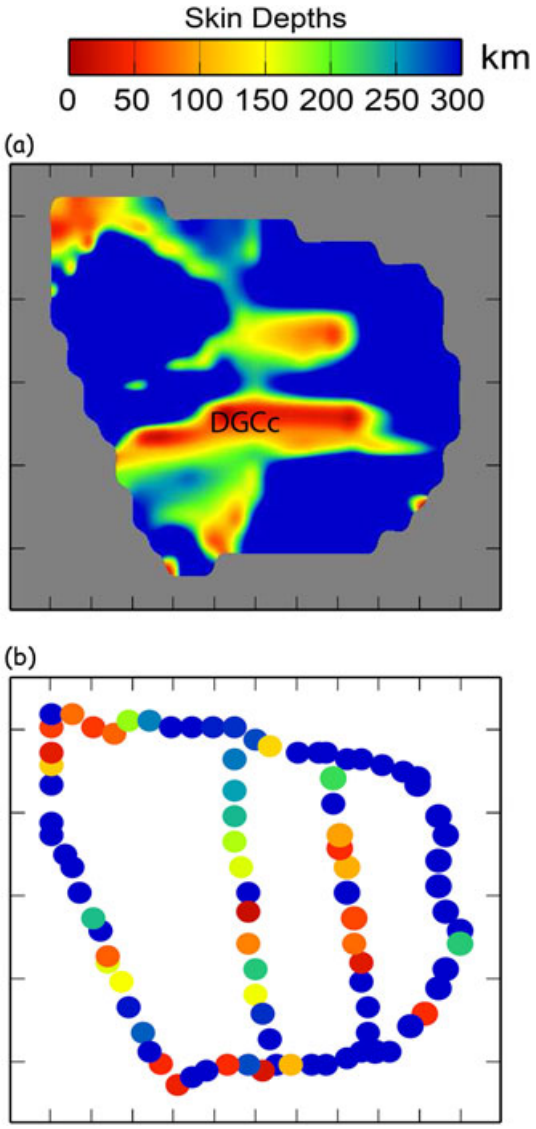

Figure 13. (a) Depth of penetration interpolated across the 3-D area and (b) shown for each station. It should be noted that Figure 13a is a gridded (minimum curvature) version of Figure 13b, and these are shown here to illustrate the diminished depth of penetration differences between craton blocks and the mobile belt. To this effect, the Central Damara conductor (DGCc), which displays limited penetration, is particularly distinct on the image.

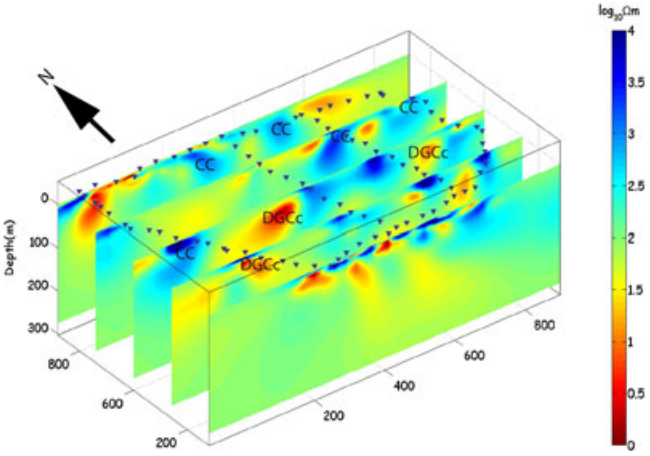

Figure 14. Perspective view of 3-D inversion model, with E-W slices across the modeled space. CC: Congo craton, DGCc: Damara Ghanzi-Chobe conductor. The inverted triangles shows the locations of the MT sites.

[32] The upper crustal resistive features are mapping the syntectonic and posttectonic granitic intrusions that form a significant component of the Damara belt outcrops, particularly in the Central Zone.

[33] Also evident in the MT model is the presence of the lower crustal conductive feature described previously [*van Zijl and de Beer*, 1983; *Ritter et al.*, 2003]. The 3-D inversion results suggest that the DGC conductor is extensive along strike of the Damara orogen, as is evident on the depth slices (Figure 10). Spatial comparison with geological maps suggests that this conductor resides mainly in the Central Zone of the DGC, the top of which is at approximately 20 km. The depth to the base of the conductive feature is generally poorly resolved due to the inductive nature of the MT technique and the limited penetrative ability of the EM fields below conductors.

[34] The Kamanjab Inlier, which forms the basement upon which Damara sediments were deposited circa 770 Ma, is imaged as a very resistive feature. Compositionally, the Kamanjab inlier comprises granotoids and metarmorphic sequences [*Goscombe et al.*, 2003], which accounts for its high resistivity (over 10,000 Ωm). The surface boundary of the inlier is traced on the geological map between sites ETO011 and ETO012; however, the MT model reveals that this boundary could be extended even further south between ETO009 and ETO010. Furthermore, the boundary of the Kamanjab Inlier at depth appears to have a gentle dip to the south, terminating beneath the Damara north Central Zone.

[35] The Autseib Lineament (AL) is one of the most prominent magnetic anomalies in the Southern Africa [*Corner*, 2008]. It separates the Damara Central Zone from the Northern Zone and extends northwestward into Botswana (see Figure 2). The AL, a former extensional fault reactivated as recently as the Mesozoic [*Clemenson et al.*, 1997; *Corner and Swart*, 1997], is now a thrust fault and

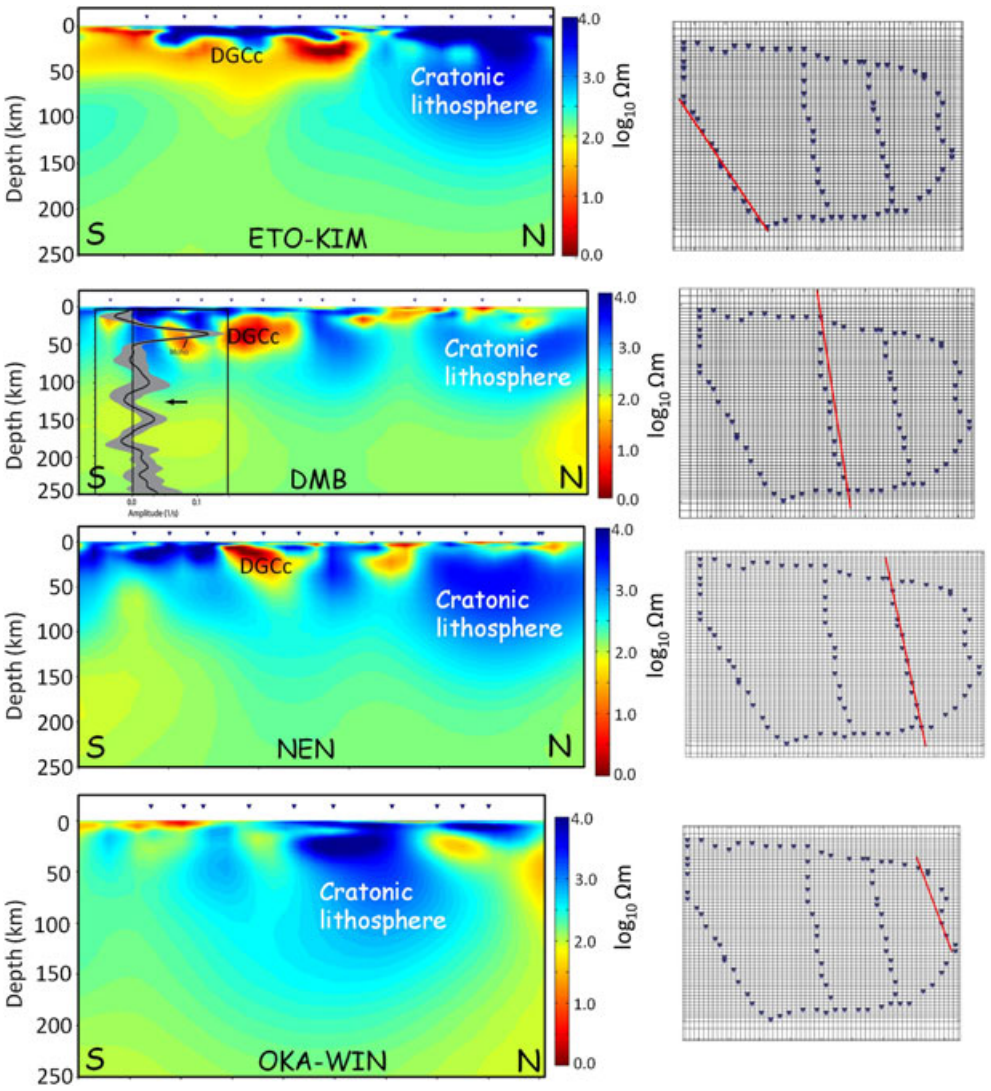

Figure 15. Two-dimensional profiles of ETO-KIM, DMB, NEN, and OKA-WIN transects extracted from 3-D inversion model. Profile locations derived are shown beside each image. The *S*-receiver function response is projected on the DMB profile as it is in closest proximity. The interpreted MOHO and LAB conversions, the latter indicated by a black arrow from *Kumar et al.* [2007], are shown. The LAB conversion (180 km) derived by *Hansen et al.* [2009] was not particularly well resolved as the signal at these depths is close to bootstrap error limits (2σ).

appears on the resistivity model as an upper crustal conductor, steeply dipping to the south. Evidence for modern reactivation along the preexisting feature was presented by *Raab* [2002] using apatite fission results.

7.2. Mantle Lithosphere

[36] Figure 11 shows the (a) isotropic and (b–c) anisotropic lithospheric scale 2-D models derived for the ETO-KIM profile. The smooth electrical resistivity models reveal a heterogeneous electrical resistivity for the mantle lithosphere. The Damara belt crustal conductor remains evident in the lithospheric model, as well as the resistive crustal granitoids. The most striking feature on the MT models is the resistive (i.e., colder), thicker lithosphere interpreted to be the electrical manifestation of the southern Congo craton. The resistivity of the cratonic segment ranges from 5000 Ωm to over 30,000 Ωm at 100 km depths, consistent with laboratory-derived dry olivine resistivities [*Constable et al.*, 1992; *Jones et al.*, 2009; *Fullea et al.*, 2011]. The southernmost extent of the Congo craton lithosphere is prominent and at a depth of about 150 km directly beneath the Autseib lineament, where there is significant change in resistivity from 30,000 Ωm to about a 1000 Ωm.

[37] The anisotropic models suggest elevated mantle conductivities in directions parallel to the profile (R_{yy}, particularly for the lowermost mantle beneath the Congo craton. As mentioned above, various candidates for mantle anisotropy include (but are not limited to) strain-induced crystal preferred orientation (CPO) of anisotropic minerals, hydrogen diffusivity in mantle minerals, and/or the presence of partial melt [*Wannamaker*, 2005; *Yoshino et al.*, 2006]. Due to the lack of mantle xenoliths samples and

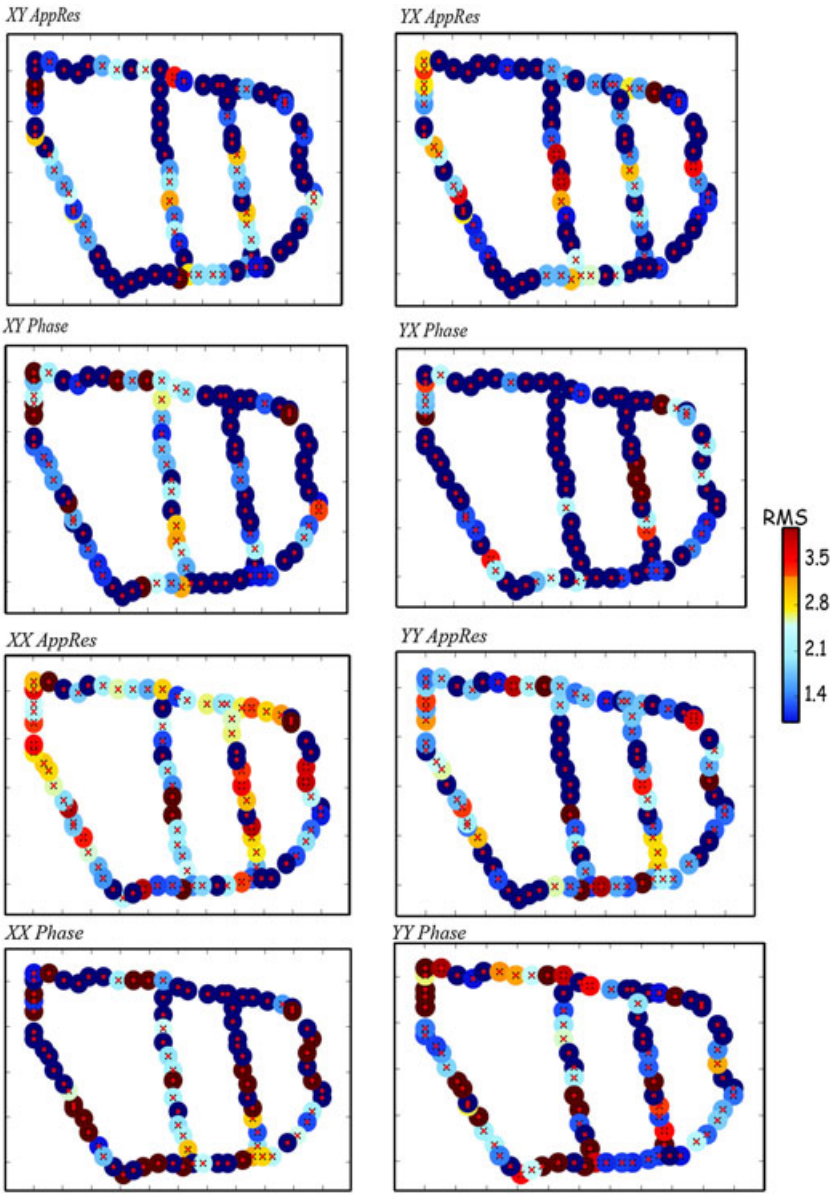

Figure 16. Variation in RMS for all the components of the impedance tensor, depicting the confidence level across the 3-D block. Most stations returned a relatively good fit with a low RMS of less than 2, particularly the diagonal elements (Z_{xy} and Z_{yx}) and their corresponding phase responses.

age dates in the northern Namibia region (though there are kimberlites), it is unknown (to us) if the mantle is dominated by hartzburgite, lherzolite, or dunite. Xenolith-defined temperature profiles derived in the Kundelungu plateau in the Democratic Republic of Congo (NE of Namibia) suggest that the Congo craton lithosphere experienced melt-induced metasomatic episodes [*Batumike et al.*, 2009] circa 32 Ma ago with lithosphere-asthenosphere boundary (LAB) depths estimated at 175 km. This result is consistent with a recent thermobarometric study of *Ashchepkov et al.* [2011], who analyzed mantle xenocrysts from the Catoca kimberlite cluster in northern Angola, and inferred a geotherm of 37–40 mWm^{-2} and a fertile clinopyroxene-rich layered mantle lithosphere with metasomatic signatures. If these geothermal conditions are representative for the larger Congo craton lithosphere to the south in Namibia, then it is reasonable to expect a slightly hydrated lower mantle lithosphere, which could explain the enhanced conductivities. This would though be in sharp contrast to the Kaapvaal Craton, which has a hydrated upper lithosphere and a dry lower lithosphere [*Peslier et al.*, 2010]. Furthermore, given its lower geothermal gradient profile, it can inferred that the Congo craton lithosphere must be thicker at its core than, say the Kaapvaal craton lithosphere, as the latter shows a slightly elevated geotherm of 41–44 mWm^{-2} (see results of *Muller et al.* [2009]).

[38] Figure 12 shows the ETO-KIM and *Muller et al.* [2009] KIM-NAM profiles, depicting the current tectonic

geometry derived from modeling MT data. Major Archean cratonic segments (Kaapvaal and Congo) are delineated from Proterozoic (Rehoboth Terraine) and Neoproterozoic (Damara belt) regions by their thickness and resistivities, confirming again the general correlation of older lithosphere being thick and resistive, whereas younger lithosphere is thin and shows elevated conductivity.

[39] Due to the extensive regional size of the study area, it is important to estimate the depth of investigation at all the stations in order to gain confidence in the derived 2-D and 3-D models. Figure 13a shows the maximum Niblett-Bostick penetration depths interpolated across the 3-D data space, with the Central Damara conductor being most prominent as it results in limited penetration of EM fields. Generally, for most stations, penetration depths were in excess of 200 km (Figure 13b). It must be recognized that the penetration depths are only from a 1-D approach but give a qualitatively accurate view.

[40] Figure 14 shows a perspective view of the 3-D inversion result as N-S profiles across the model block. The thick resistive Congo craton (CC) lithosphere is clearly mapped, including the Central Damara belt conductor (DGCc). In order to obtain an indication of the variation in geometry of the tectonic features across the region, 2-D profiles were extracted out of the 3-D inversion model, and the results are shown in Figure 15 for the ETO-KIM, DMB, NEN, and OKA-WIN profiles from west to east. The TSUM *S* wave receiver function site is also shown on the DMB profile.

[41] The nature of 3-D inversion is such that more data (i.e., full impedance tensor) are modeled; as a result, one expects the 2-D and 3-D results to differ (Figure 15). Additionally, variable grid size, lack of data, misfit distribution, and trade-off parameter will introduce variations in the models. The geometric variations of cratonic lithosphere observed between the profiles could be the result of this very fact. That being the case, the general features of the model that are robust are the cratonic lithosphere to the north and the presence of the Central Damara conductor, which were also observed in the 2-D models. The modeled responses fit the observed data well, as illustrated in Figure 16, which shows the RMS difference for all impedance tensor elements of the modeled responses and the resulting 3-D inversion model.

8. Discussion

8.1. Crustal Model

[42] The resistive granitic plutons comprise a significant percentage of the geological outcrop of the Central Zone and reflect massive amounts of volcanism [*Gray et al.*, 2007]. There are three plausible mechanisms that could result in huge voluminous melt generation specific to the Damara Belt Central Zone: (1) volcanism generated during the initial 750 Ma rifting phase, (2) decompression melting of subducted Khomas oceanic lithosphere (560 Ma), and/or (3) melt derived from crustal recycling of turbiditic material during final 540–520 Ma collision [*Gray et al.*, 2007]. Isotopic studies on granites [*McDermott et al.*, 2000; *Jung and Mezger*, 2003], however, indicate that the granites in the Central Zone lack positive mantle signatures (i.e., positive ε_{Nd}, low $\delta^{18}O$). S-type granites, which are particularly most significant in volume in the Central Zone, have similar chemical and isotopic signatures to the Neoproterozoic turbidites in the southern zone, indicating a fertile "turbiditic" crustal source at midcrustal levels by dehydration melting [*Gray et al.*, 2007].

[43] *Jung and Mezger* [2003] and *McDermott et al.* [2000] suggest that the Damara Central Zone, which has high thermal gradients (30–50°C/km) and high-temperature/moderate-pressure metamorphic conditions, underwent significant middle to lower crustal low-pressure melting that generated the voluminous posttectonic granites imaged by the MT model. The elevated gradients correlate with the observed conductivity structure of the Damara Central Zone. More subdued geothermal gradients are observed in the Barrovian metamorphism-dominated marginal zones of the north and southern Damara belt.

[44] The detection of the well-known crustal conductor in the Damara belt still requires explanation, as its understanding and characterization has tectonic implications. Issues that still need attention regarding this conductor include its possible causes and, most importantly, its apparent spatial along-strike extent. These will be addressed now.

[45] *Ritter et al.* [2003] attributed graphite along fossilized shear zones as the cause of the observed conductor, based on field evidence of graphite-bearing marble units. Geological exposures indicate the presence of accessory sulfides and oxides (Ben Goscombe, personal communication, 2012) which could explain the presence of conductive anomalies in the DGC upper crust. Massive sulfide mineralization (Cu-Zn-Au) is also found, for example, in the Matchless Amphibolite belt in the Damara Southern Zone; the latter being thought to represent a possible relict oceanic lithosphere [*Barnes and Sawyer*, 1980]. This observation suggests that sulfides could have been introduced in the Damara crust in the same manner (subduction) as for the longest-known crustal conductivity anomaly, namely, the North American Central Plains (NACP) conductor [*Jones et al*., 1993, 2005b]. Furthermore, if the Matchless Amphibolite represents fossil oceanic lithosphere, it is reasonable to expect the presence of carbon in graphite form, which would elevate the conductivity significantly as it would provide an efficient conduction mechanism. It is worth noting that high heat flow is also associated with crustal conductors in the Wopmay orogen [*Wu et al.*, 2005] and in the Trans-Hudson Orogen [*Jones et al.*, 1993].

[46] While hydrothermal crustal fluids could be present in the middle to lower crust, it is highly unlikely to give rise to the high conductivities observed due to their relatively short residence times in the crust [*Bailey*, 1990] and lack of supporting field evidence of alteration. Thus, a combination of graphite and sulfides offer the most plausible explanation for the increased conductivity in the Damara Central Zone.

[47] The apparent large strike extent of the Central Zone conductor could be a result of regional metamorphic processes or structural placement of interconnected graphite/sulfides and speaks to coherent along-strike tectonic processes, as for the NACP above. The DGC Central Zone is a high-temperature/low-pressure metamorphic zone, bounded to the north and south by zones of intermediate temperature and pressure metamorphism, which define regions of structural thickening [*Maloof*, 2000; *Gray et al.*, 2007]. It is possible that during periods of

accretion and marked shortening thickening, graphite was preferentially emplacement along grain boundaries, and deep shear movement facilitated graphite interconnectivity, an argument that was also invoked by *Ritter et al.* [2003]. This argument is supported by *Kisters et al.* [2004], who observed that during peak high-temperature/low-pressure metamorphism (circa 538–505 Ma), the central Damara zone underwent pure shear deformation with lateral-parallel orogen stretch. Furthermore, microscopic investigations [*Walter*, 2004] in the DGC Central Zone reveal that graphite shows a strong lattice-preferred orientation in the mylonitic core zones. This strain-induced graphite, which might have been concentrated during collision of Congo and Kalahari cratons, would explain the large lateral (along strike) extent of the observed conductivity anomalies.

[48] In summary, combining the electrical and metamorphic observations, the abundance of resistive S-type granites in the high-temperature Central Zone resulted from remelting of turbidites, facilitated by magmatic under-plating at lower crust levels, during the final collisional phase of the Congo and Kalahari cratons. The conductivity in the middle to lower crust appears to have multiple possible causal sources, with graphite along deep-seated shear zones being the most probable and sulfide mineralization being more dominant in the upper crust.

8.2. Mantle Lithosphere

[49] Mantle electrical resistivity is more sensitive to temperature variations than it is to composition [*Jones et al.*, 2009]; thus, "colder" and thicker cratonic lithosphere are generally well-imaged with the MT method and can be distinguished from "warmer," generally thinner, mobile belts. The top of conductive zones overlain by resistive features, such as the boundary between cratonic lithosphere and asthenosphere, can be efficiently imaged to within 10% with high-quality MT data [*Jones*, 1999]. For smoother models, such as those derived in our case, the lithosphere-asthenosphere transition is not sharply defined, but rather appears as a broad gradational boundary as consequence of smooth regularization.

[50] There are several definitions of what the LAB is (see, for example, *Eaton et al.* [2009]). Mantle adiabatic temperature and composition will determine the electrical conductivity of the asthenosphere [*Evans et al.*, 2011], but for a completely dry peridotitic rigid lithosphere, the onset of the transition to asthenospheric conditions tends to occur at conductivities in the order of 10^{-2} S/m and greater (global averages are for conductivities of order 0.04–0.2 S/m for the asthenosphere) [*Jones*, 1999]. While this transition is not sharply imaged for the central Damara belt, due to the shielding effect of the conductive mid-lower crust, for sites outside this conductive zones, where depth of penetration is assured, the boundary appears to be at depths of around 160 km. Similar depth estimates were found by *Muller et al.* [2009]. *Fishwick* [2010] estimated, from surface wave tomographic models, lithospheric thickness in the range 160–180 km from the DGC. The DGC's signal for the lithosphere-asthenosphere boundary (LAB) from the SRFs at station TSUM is not well resolved, due to high 2σ error bounds, but is nevertheless estimated at 180 ± 20 km (see Figure 15 for the DMB profile). Thus, all three methods, MT, surface wave tomography, and SRF, give an LAB of 160–180 km. Forward modeling was carried out to test the resolution of the features in the model. This was done by various ways including locking some cells of features in the model and noticing appreciable changes in the RMS. Furthermore, some features, like cratonic lithosphere, were painted with 100 Ωm and the result inverted. The return of the feature in the inversion proved that cratonic segments are required by the model and depth estimates remained the same. Mantle xenoliths, showing lherzolitic and harzburgitic composition, found in the Cretaceous nephelinite plug within the Central Zone of the DGC, 17 km east of Swakopmund, suggest an elevated geotherm (90 mW/m^2 from *Whitehead et al.* [2002]) which is significantly higher than the Rehoboth Terrane (45 mW/m^{-2} from *Muller et al.* [2009]). This composition is typical for Proterezoic mantle. The elevated geothermal gradient in the Damara belt is possibly related to the postcollisional tectonothermal events, evidence of which is widespread and in the form of granites particularly in the Central Zone. Furthermore, *Whitehead et al.* [2002] infers a heterogeneous, oxidized, and fertile-to-refractory mantle beneath Damara Central Zone. The xenolith geotherm is, however, based on relatively few samples and, if representative at all, reflects upper lithospheric mantle temperatures at the time of kimberlite eruption (75 Ma) suggesting lateral temperature and lithospheric thickness variations from the Rehoboth (180 km) to the DGC (160 km). As geochemical and age constraints for the DGC lithospheric mantle are absent, our data and results provide no constraints on whether the DGC lithospheric mantle might consist of a younger component, created and stabilized coeval with Pan-African orogenesis.

[51] What is immediately clear is that the envisaged boundary of the Congo craton by *Corner* [2008] and *Begg et al*. [2009] does not correlate with the mapped extension of the cratonic lithosphere from the electrical resistivity results. These authors have the margin close to MT station NEN022 on the NEN profile (Figure 3). The resistivity model suggests that this margin is approximately 100 km further south, close to station NEN118, and has a steep southward dip up to 80 km depth. The Tsumkwe (in Namibia) and Nxa-Nxau kimberlite fields on the border between Namibia and Botswana (see Figure 3) are located on an area of resistivity gradients which spatially correlates with lithospheric thickness change from a thinner mobile belt to a thicker craton (see the NEN model, for example). A similar trend was remarked upon by *O'Neill et al.* [2005] and *Jones et al*. [2009] where, in general, diamondiferous kimberlites appear to occur on areas of lateral resistivity and velocity gradients at the edges of cratons, indicating shallowing of lithospheric roots.

[52] The Okavango Dyke Swam (ODS), which crosses the OKA-WIN profile at an area between OKA008 and OKA004, is imaged as a resistive feature on this profile. Compositionally, the ODS is made up of dolerite dykes of varying widths ranging from 0.2 to 67 m, which *Miensopust et al.* [2011] showed manifest themselves as an anisotropic feature in 2-D models. The ODS is hosted in similarly resistive granite-gneiss host rocks, such as the Kwando complex, the Rooibok Complex (analogous to Matchless Amphibolite in Namibia) and various Paleoproterozic igneous basements obscured by younger strata (though magnetically distinct). Thus, while its field outcrops is well constrained, it is

not readily distinguishable from its resistive hosts on the MT model.

8.3. Rifting in the Okavango Delta?

[53] There has been some suggestions that the East African Rift System extends into northwestern Botswana, based on persistent seismicity [*Reeves*, 1972], forward modeling of magnetic and gravity data [*Kinabo*, 2007], and anomalous heat flow [*Chapman and Pollack*, 1974]. All geophysical experiments done on the Okavango Rift Zone (ORZ), before ours, focused on shallow (less than 1 km) structure [*Modisi et al.*, 2000; *Kinabo*, 2007; *Bufford et al.*, 2012] and revealed the ORZ as a half-graben feature. If indeed continental rifting is taking place, then one might expect a classic rift signature of thinned lithosphere accompanied by a localized deep-seated high conductivity mantle anomalies, as is observed, for example, in the Rio Grande Rift [*Hermance and Pedersen*, 1980; *Jiracek et al.*, 1983; *Hermance and Neumann*, 1991]. None of these features is observed on the electrical resistivity models, particularly along the OKA-WIN profile. The lack of elevated mantle conductivity suggests that incipient continental rifting, if taking place, is generated from preexisting structural features in the crust, as proposed by *Birt et al.* [1997] for the Kenya Rift, and propagates downward without any mantle upwelling signature.

8.4. Congo Craton Southern Extent

[54] In general, the MT models suggest that the Congo craton lithosphere extends significantly southward beneath the Northern Platform sequences of Damara belt. The southern and northern DGC passive margin sequences, which were deposited on a rift margin, appear to be overthrusted onto both cratonic nuclei during continental amalgamation at 495 Ma, supporting studies by *Goscombe* [2004], to give a doubly vergent orogen. This result means that the current tectonic lines mapping the southern edge of the Congo craton need to be revised and drawn further south.

[55] It is interesting to note the striking similarity between our MT models and other Archean-Proterozoic margins around the world in imaging steeply conductive features separating the two terrains. For example, the Central Australian Suture Zone, which forms the contact between the North Australian craton and the Proterozoic Warumpi province [*Selway et al.*, 2006, 2009], is mapped as a dipping conductor. Also, in Australia, the Errabiddy Shear Zone forms a conductive suture between the Yilgarn Craton and the Glenburgh Terrane [*Selway et al.*, 2009]. The margin between the Slave craton and the Wopmay orogen [*Spratt et al*., 2009] is preserved as steeply dipping conductive structure. All of these features were subjected to later reactivation postcontinental collision. This observation suggests that steeply dipping crustal-scale conductive structures can be used to infer continental accretion, and perhaps, broad generalization can be inferred about similar mode of evolution for Archean/Proterozoic margins.

9. Conclusions

[56] The three dominant features evident in the 2-D and 3-D MT models are (i) the Pan-African granitic plutons, (ii) the mid-lower crustal conductor of the Damara belt, and (iii) the thick resistive lithosphere of the southern Congo craton. The DGC is thought to have experienced a full Wilson cycle, involving initial continental rifting (770–746 Ma) leading to the development of the Khomas sea basin at 770 Ma, followed by the subduction closing of Khomas ocean. The presence and spatial extent of Congo cratonic lithosphere was mapped in northern Namibia for the first time using magnetotelluric data. The two-dimensional resistivity models reveal features which correlate with known structural and lithologic features. The upper crust of the DGC is characterized by both resistive and conductive structures, the former interpreted to be granitic intrusions in the Central Zone related to the Pan-African magmatic events. A middle to lower crustal conductor is confirmed, the origin of which is observed in the DGC which we propose to be related preferential alignment of graphitic/sulfide materials during the collision of Kalahari and Congo cratons as part of Gondwana amalgamation.The southward steeply dipping structure (corresponding to the Autseib Lineament) we propose is a feature that is distinct to Archean/Proterozoic margins and that it should be used to target and distinguish terranes of different ages.

[57] The MT models constrain the previously unknown position and geometry of the southern Congo craton at depth and provide the first electrical resistivity map of the crustal and mantle lithosphere beneath this previously unknown boundary. The lack of mantle signature typically associated with rifts is not observed in the MT models which suggest that if indeed incipient rifting is taking place in northwestern Botswana, the process is initiated from surface downward.

[58] **Acknowledgments.** The SAMTEX consortium members (Dublin Institute for Advanced Studies, Woods Hole Oceanographic Institution, Council for Geoscience (South Africa), De Beers Group Services, The University of the Witwatersrand, Geological Survey of Namibia, Geological Survey of Botswana, Rio Tinto Mining and Exploration, BHP Billiton, Council for Scientific and Industrial Research (South Africa), and ABB Sweden) are thanked for their funding and logistical support during the four phases of data acquisition. Other members of the SAMTEX team include: L. Collins, C. Hogg, C. Horan, G. Wallace, M. Miensopust (DIAS), A. D. Chave (WHOI), J. Cole, P. Cole, R. Stettler (CGS), T. Ngwisanyi, G. Tshoso (GSB), D. Hutchins, T. Katjiuongua (GSN), E. Cunion, A. Mountford, T. Aravanis (RTME), W. Pettit (BHPB), H. Jelsma (De Beers), P.-E. Share (CSIR), and J. Wasborg (ABB).

[59] This work is also supported by research grants from the National Science Foundation (EAR-0309584 and EAR-0455242 through the Continental Dynamics Program to R. L. Evans), the Department of Science and Technology, South Africa, and Science Foundation of Ireland (grant 05/RFP/ GEO001to A. G. Jones). The magnetic data courtesy of the Council for Geoscience South Africa. The Irish Centre for High Performance Computing (ICHEC) is thanked for availing the STOKES cluster to carry out the numerical computations. Gary Egbert and Weerechaii Siripunvarapon are thanked for providing, respectively, the ModEM and WSINV3DMT codes and Naser Meqbel and Jan Vozar for installing the code on our clusters. Some figures in the paper are plotted using the Generic Mapping Tools (GMT) of *Wessel and Smith* [1991] and *Wessel and Smith* [1998].

References

Anamte, C., and B. W. Eakins, (2009), Etopo1 arc-minute global relief model: Procedures, data sources and analysis, *Tech. rep.*, NOAA.

Ashchepkov, I., et al. (2011), Composition and thermal structure of the lithospheric mantle beneath kimberlite pipes from the Catoca cluster, Angola, *Tectonophysics*, *530–531*, 128–151, doi:10.1016/j.tecto.2011.12.007.

Baba, K., P. Tarits, A. D. Chave, R. L. Evans, G. Hirth, and R. L. Mackie (2006), Electrical structure beneath the northern MELT line on the East Pacific Rise at 1545'S, *Geophys. Res. Lett.*, *33*, L22301, doi:10.1029/2006GL027528.

Bahr, K., and A. Duba (2000), Is the asthenosphere electrically anisotropic? *Earth Planet. Sci. Lett.*, *178*, 87–95.

Bailey, R. C. (1990), Trapping of aqueous fluids in the deep crust, *Geophys. Res. Lett.*, *17*, 1129–1132.

Barnes, S., and E. Sawyer (1980), An alternative model for the Damara mobile belt: Oceanic crust subduction and continental convergence, *Precambrian Res.*, *13*, 297–336.

Batumike, J., W. Griffin, and S. O'Reilly (2009), Lithospheric mantle structure and the diamond potential of kimberlites in southern D.R. Congo, *Lithos*, *112*, 166–176, doi:10.1016/j.lithos.2009.04.020.

Begg, G. C., et al. (2009), The lithospheric architecture of Africa: Seismic tomography, mantle petrology, and tectonic evolution, *Geosphere*, *5*, 23–50, doi:10.1130/GES00179.1.

Birt, C., P. Maguire, M. Khan, H. Thybo, G. Keller, and J. Patel (1997), The influence of pre-existing structures on the evolution of the southern Kenya Rift Valley-evidence from seismic and gravity studies, *Tectonophysics*, *278*(1-4), 211–242, doi:10.1016/S0040-1951(97)00105-4.

Bostick Jr., F. X. (1977), A simple almost exact method of magnetotelluric analysis: Proc. Workshop on electrical methods in geothermal exploration, U.S. Geological Survey, 174–183.

Bufford, K. M., E. a. Atekwana, M. G. Abdelsalam, E. Shemang, E. a. Atekwana, K. Mickus, M. Moidaki, M. P. Modisi, and L. Molwalefhe (2012), Geometry and faults tectonic activity of the Okavango Rift Zone, Botswana: Evidence from magnetotelluric and electrical resistivity tomography imaging, *J. Afr. Earth. Sci.*, *65*, 61–71, doi:10.1016/j.jafrearsci.2012.01.004.

Chapman, S., and N. Pollack (1974), Heat flow and heat production in Zambia: Evidence for lithospheric thinning in central Africa, *Tectonophysics*, *41*, 79-100.

Chave, A. D., and A. G. Jones (2012), *The Magnetotelluric Method: Theory and Practice*, 570 pp., Cambridge University Press, New York.

Clemenson, J., J. Cartwright, and J. Booth (1997), Structural segmentation and the influence of basement structure on the Namibian passive margin, *J. Geol. Soc.*, *154*(3), 477–482, doi:10.1144/gsjgs.154.3.0477.

Constable, S., T. J. Shankland, and A. Duba (1992), The electrical conductivity of an isotropic olivine mantle, *J. Geophys. Res.*, *97*(B3), 3397–3404, doi:10.1029/91JB02453.

Corner, B. (2008), Crustal framework of Namibia derived from an integrated interpretation of geophysical and geological data, in *The Geology of Namibia: Archean to Mesoproterozoic, Special Publication of the Geol. Survey of Namibia,* vol. 1, edited by R. M. G. Miller, pp. 1–19, Geological Survey of Namibia, Windhoek.

Corner, B., and R. Swart (1997), Structural insights gained from comparison of offshore Namibia satellite data with onshore magnetic and gravity data, in *Proceedings of the 5th Meeting of the South African Geophys. Ass.*, pp. 173–174, South African Geophysical Association, SAGA, Swakopmund, poster presented at Poc. 5th Meeting of SAGA, Swakopmund.

Daly, M. C. (1986), Crustal shear zones and thrust belts: Their geometry and continuity in central Africa, *Philos. Trans. Roy. Soc. London*, *317*, 111–128.

Davis, W. (2003), Lithosphere development in the Slave craton: A linked crustal and mantle perspective, *Lithos*, *71*(2-4), 575–589, doi:10.1016/S0024-4937(03)00131-2.

de Beer, J. H., D. I. Gough, and J. S. V. van Zijl (1975), An electrical conductivity anomaly and rifting in southern Africa, *Nature*, *255*(5511), 678–680, doi:10.1038/255678a0.

de Beer, J. H., J. S. V. van Zijl, R. M. J. Huyssen, P. L. V. Hugo, S. J. Joubert, and R. Meyer (1976), A magnetometer array study in south-west Africa, Botswana and Rhodesia, *Nature*, *45*, 1–17.

de Beer, J. H., R. M. J. Huyssen, S. J. Joubert, and J. S. V. Van Zijl (1982), Magnetometer array studies and deep Schlumberger soundings in the Damara Orogenic Belt, South West Africa, *Geophys. J. R. Astron. Soc.*, *70*(1), 11–29, doi:10.1111/j.1365-246X.1982.tb06388.x.

Duba, A., S. Heikamp, W. Meurer, G. Mover, and G. Will (1994), Evidence from borehole samples for the role of accessory minerals in lower-crustal conductivity, *Nature*, *367*(6458), 59–61, doi:10.1038/367059a0.

Eaton, D. W., A. G. Jones, and I. J. Ferguson (2004), Lithospheric anisotropy structure inferred from collocated teleseismic and magnetotelluric observations: Great Slave Lake shear zone, northern Canada, *Geophys. Res. Lett.*, *31*, L19614, doi:10.1029/2004GL020939.

Eaton, D. W., F. Darbyshire, R. L. Evans, H. Grütter, A. G. Jones, and X. Yuan (2009), The elusive Lithosphere Asthenosphere Boundary (LAB) beneath cratons, *Lithos*, *109*, 1–22, doi:10.1016/j.lithos.2008.05.009.

Egbert, G. D., and J. R. Booker (1986), Robust estimation of geomagnetic transfer functions, *Geophys. J. R. Astron. Soc.*, *87*(1), 173–194, doi:10.1111/j.1365-246X.1986.tb04552.x.

Egbert, G. D., and A. Kelbert (2012), Computational recipes for electromagnetic inverse problems, *Geophys. J. Int.*, *189*, 251–267, doi:10.1111/j.1365-246X.2011.05347.x.

Evans, R. L. et al. (2011), Electrical lithosphere beneath the Kaapvaal Craton, Southern Africa, *J. Geophys. Res.*, *116*, B04105, doi:10.1029/2010JB007883.

Evans, S., A. G. Jones, J. Spratt, and J. Katsube (2005), Central Baffin Electromagnetic Experiment (CBEX): Mapping the North American Central Plains (NACP) conductivity anomaly in the Canadian arctic, *Phys. Earth Planet. Int.*, *150*, 107–122, doi:10.1016/j.pepi.2004.08.032.

Farquharson, C. G., and J. A. Craven (2009), Three-dimensional inversion of magnetotelluric data for mineral exploration: An example from the McArthur River uranium deposit, Saskatchewan, Canada, *J. Appl. Geophys.*, *68*, 450–458, doi:10.1016/j.jappgeo.2008.02.002.

Fernàndez, M., J. Afonso, and G. Ranalli (2010), The deep lithospheric structure of the Namibian volcanic margin, *Tectonophysics*, *481*, 68–81, doi:10.1016/j.tecto.2009.02.036.

Fishwick, S. (2010), Lithos Surface wave tomography: Imaging of the lithosphere asthenosphere boundary beneath central and southern Africa, *Lithos*, *120*, 63–73, doi:10.1016/j.lithos.2010.05.011.

Frimmel, H. (1998), Neoproterozoic tectono-thermal evolution of the Gariep Belt and its basement, Namibia and South Africa, *Precambrian Res.*, *90*(1-2), 1–28, doi:10.1016/S0301-9268(98)00029-1.

Fullea, J., M. R. Muller, and A. G. Jones (2011), Electrical conductivity of continental lithospheric mantle from integrated geophysical and petrological modeling: Application to the Kaapvaal Craton and Rehoboth Terrane, Southern Africa, *J. Geophys. Res.*, *116*, B10202, doi:10.1029/2011JB008544.

Gamble, T. D., W. M. Goubau, and J. Clarke (1979), Magnetotellurics with a remote reference, *Geophysics*, *44*, 53–68.

Gatzemeier, A., and A. Tommasi (2006), Flow and electrical anisotropy in the upper mantle: Finite-element models constraints on the effects of olivine crystal preferred orientation and microstructure, *Phys. Earth Planet. Inter.*, *158*, 92–106, doi:10.1016/j.pepi.2006.01.009.

Goscombe, B. (2004), Variation in metamorphic style along the Northern Margin of the Damara Orogen, Namibia, *J. Petrol.*, *45*, 1261–1295, doi:10.1093/petrology/egh013.

Goscombe, B., M. Hand, D. Gray, and J. Mawby (2003), The metamorphic architecture of a transpressional orogen: The Kaoko Belt, Namibia, *J. Petrol.*, *44*(4), 679–711, doi:10.1093/petrology/44.4.679.

Gray, D. R., D. A. Foster, B. D. Goscombe, R. A. Trouw, and C. W. Passchier (2006), 40ar/39ar thermochronology of the Pan-African Damara Orogen, Namibia, with implications for tectonothermal and geodynamic evolution, *Precambrian Res.*, *150*, 49–72, doi:10.1016/j.precamres.2006.07.003.

Gray, D. R., D. A. Foster, J. G. Meert, B. D. Goscombe, R. Armstrong, R. A. Trouw, and C. W. Passchier (2007), Continental growth and recycling by accretion of deformed turbidite fans and remnant ocean basins: Examples from neoproterozoic and phanerozoic orogens, *Mem. 200: 4-D Framework of Cont. Crust*, *200*, 63–92, doi:10.1130/2007.1200(05).

Gray, D. R., D. A. Foster, J. G. Meert, B. D. Goscombe, R. Armstrong, R. A. Trouw, and C. W. Passchier (2008), A Damara orogen perspective on the assembly of Southwestern Gondwana, *Geol. Soc. Lond. Spec. Publ.*, *294*, 257–278, doi:10.1144/SP294.14.

Griffin, W. L., S. Y. O'Reilly, N. Abe, S. Aulbach, R. M. Davies, N. J. Pearson, B. J. Doyle, and K. Kivi (2003), The electrical resisitivty log as an aid to determining some resevoir characteristics, *Precambrian Res.*, *127*, 19–41.

Groom, R. W., and R. C. Bailey (1989), Decomposition of magnetotelluric impedance tensors in the presence of local three-dimensional galvanic distortion, *J. Geophys. Res.*, *94*, 1913–1925.

Hamilton, M. P., A. G. Jones, R. L. Evans, S. Evans, C. J. S. Fourie, X. Garcia, A. Mountford, J. E. Spratt, and S. M. Team (2006), Electrical anisotropy of South African lithosphere compared with seismic anisotropy from shear-wave splitting analyses, *Phys. Earth Planet. Int.*, *158*, 226–239, provided by the SAO/NASA Astrophysics Data System.

Hansen, P. C., and D. P. O'Leary (1993), The use of the L-Curve in the regularization of discrete ill-posed problems, *SIAM J. Sci. Comput.*, *14*(6), 1487–1503, doi:10.1137/0914086.

Hansen, S. E., A. A. Nyblade, and J. Julia (2009), Estimates of crustal and lithospheric thickness in sub-Saharan Sfrica from S-wave receiver functions, *S. Afr. J. Geol.*, *112*, 229–240, doi:10.2113/gssajg.112.3-4.229.

Hanson, R. E. (2003), Proterozoic geochronology and tectonic evolution of Southern Africa, in *Proterozoic East Gondwana: Supercontinent Assembly and Breakup*, edited by Yoshida, M., B. Windley, and S. Dasgupta, pp. 427–463, Geological Society of London Special Publication, London.

Hermance, J. F., and G. A. Neumann (1991), The Rio Grande rift: New electromagnetic constraints on the Socorro magma body, *Phys. Earth Planet. Inter.*, *66*(1-2), 101–117, doi:10.1016/0031-9201(91)90107-S.

Hermance, J. F., and J. Pedersen (1980), Deep structure of the Rio Grande Rift: A magnetotelluric interpretation, *J. Geophys. Res.*, *85*(B7), 3899–3912, doi:10.1029/JB085iB07p03899.

Hoffmann, K. H. (1994), New constraints on the timing of continental breakup and collision in the Damara Belt, in *Proterozoic Crustal and Metallogenic Evolution, Abstracts of Geological Society and Geological Survey of Namibia Conference,* vol. 30, edited by M. Niall and C. McManus, p. 30, GSN, Windhoek.

Jacobs, J., S. Pisarevsky, R. J. Thomas, and T. Becker (2008), The Kalahari craton during the assembly and dispersal of Rodinia, *Precambrian Res.*, *160*, 142–158, doi:10.1016/j.precamres.2007.04.022.

James, D. E., M. J. Fouch, J. C. VanDecar, and S. van der Lee (2001), Tectospheric structure beneath southern Africa, *Geophys. Res. Lett.*, *28*(13), 2485–2488, doi:10.1029/2000GL012578.

Ji, S., S. Rondenay, M. Mareschal, and G. Senechal (1996), Obliquity between seismic and electrical anisotropies as a potential indicator of movement sense for ductile shear zones in the upper mantle, *Geology*, *24*(11), 1033, doi:10.1130/0091-7613(1996)024<1033:OBSAEA>2.3.CO;2.

Jiracek, R., P. Gustafson, S. Mitchell, G. Sciences, and S. Diego (1983), Magnetotelluric results opposing magma origin of crustal conductors in the Rio Grande Rift, *Tectonophysics*, *94*, 299–326.

Jones, A., D. Cough, R. Kurtz, J. D. D. Boerner, J. Craven, R. Ellis, and G. McNeice (1992), Electromagnetic images of regional structure in the Southern Cordillera, *Geophys. Res. Lett.*, *12*, 2373–2376.

Jones, A., et al. (2005a), The electrical resistivity structure of Archean to Tertiary lithosphere along 3200 km of SNORCLE profiles, northwestern Canada, *Can. J. Earth Sci.*, *42*, 1257–1275.

Jones, A. G. (1983), The problem of current channelling: A critical review, *Geophys. Surv.*, *6*, 79–122.

Jones, A. G. (1988), Static shift of magnetotelluric data and its removal in a sedimentary basin environment, *Geophysics*, *53*, 967–978.

Jones, A. G. (1999), Imaging the continental upper mantle using electromagnetic methods, *Lithos*, *48*(24), 57–80, doi:10.1016/S0024-4937(99)00022-5.

Jones, A. G., and J. Jodicke (1984), Magnetotelluric transfer function estimation improvement by a coherence-based rejection technique, 54th *Ann. Mtg. Soc. of Expl. Geophys.,* Atlanta, Georiga.

Jones, A. G., A. D. Chave, D. Auld, K. Bahr, and G. Egbert (1989), A comparison of techniques for magnetotelluric response function estimation, *J. Geophys. Res.*, *94*, 14,201–14,213.

Jones, A. G., J. A. Craven, G. A. McNeice, I. J. Ferguson, T. Boyce, C. Farquharson, and R. G. Ellis (1993), North American Central plains conductivity anomaly within the trans-hudson orogen in Northern Saskatchewan, *Geology*, *21*, 1027–1030.

Jones, A. G., D. Snyder, S. Hanmer, I. Asudeh, D. White, D. Eaton, and G. Clarke (2002), Magnetotelluric and teleseismic study across the snowbird tectonic zone, Canadian shield: A Neoarchean mantle suture? *Geophys. Res. Lett.*, *29*(17), 170,000–170,001, doi:10.1029/2002GL015359.

Jones, A. G., J. Ledo, and I. J. Ferguson (2005b), Electromagnetic images of the Trans-Hudson orogen: The North American Central plains anomaly revealed, *Can. J. Earth Sci.*, *42*(4), 457–478, doi:10.1139/e05-018.

Jones, A. G., R. L. Evans, and D. W. Eaton (2009), Velocity conductivity relationships for mantle mineral assemblages in archean cratonic lithosphere based on a review of laboratory data and hashinshtrikmanextremal bounds, *Lithos*, *109*, 131–143.

Jones, A. G., J. Fullea, R. L. Evans, and M. R. Muller (2012), Water in cratonic lithosphere: Calibrating laboratory-determined models of electrical conductivity of mantle minerals using geophysical and petrological observations, *Geochem. Geophys. Geosy.*, *13*, Q06010, doi:10.1029/2012GC004055.

Jung, S., and K. Mezger (2003), U-Pb garnet chronometry in high-grade rocks-case studies from the central Damara orogen (Namibia) and implications for the interpretation of Sm-Nd garnet ages and the role of high U-Th inclusions, *Contrib. Mineral. Petrol.*, *146*(3), 382–396, doi:10.1007/s00410-003-0506-6.

Karato, S. (1990), The role of hydrogen in the electrical conductivity of the upper mantle, *Nature*, *347*(6290), 272–273, doi:10.1038/347272a0.

Karato, S. (2010), Tectonophysics Rheology of the deep upper mantle and its implications for the preservation of the continental roots: A review, *Tectonophysics*, *481*(1-4), 82–98, doi:10.1016/j.tecto.2009.04.011.

Kinabo, B. D. (2007), Early structural development of the Okavango rift zone, NW Botswana, *J. Afr. Earth. Sci.*, *48*, 125–136, doi:10.1016/j.jafrearsci.2007.02.005.

Kisters, A. F., L. Jordaan, and K. Neumaier (2004), Thrust-related dome structures in the Karibib district and the origin of orthogonal fabric domains in the south central zone of the Pan-African Damara Belt, Namibia, *Precambrian Res.*, *133*, 283–303, doi:10.1016/j.precamres.2004.05.001.

Kumar, P., X. Yuan, M. R. Kumar, R. Kind, X. Li, and R. K. Chadha (2007), The rapid drift of the Indian tectonic plate, *Nature*, *449*, 894–897, doi:10.1038/nature06214.

Le Pape, F., A. G. Jones, J. Vozar, and W. Wenbo (2012), Penetration of crustal melt beyond the Kunlun Fault into Northern Tibet, *Nat. Geosci.*, *5*, 330–335, doi:10.1038/ngeo1449.

Mackie, R., and T. Madden (1993a), Conjugate direction relaxation solutions for 3-D magnetotelluric modeling, *Geophysics*, *58*, 1052–1057.

Mackie, R., and T. Madden (1993b), Three-dimensional magnetotelluric inversion using conjugate gradients, *Geophys. J. Int.*, *115*, 215–229.

Mackie, R. L., T. Madden, and P. Wannamaker (1993), Three-dimensional magnetotelluric modeling using difference equations—Theory and comparisons to integral equation solutions, *Geophysics*, *58*, 215–226.

Mackwell, S., and D. Kohlstedt (1990), Diffusion of hydrogen in olivine: Implications for water in the mantle, *J. Geophys. Res.*, *95*, 5079–5088.

Maloof, A. (2000), Superposed folding at the junction of the inland and coastal belts, Damara Orogen, in *Henno Martin Commemorative Volume: Communications of the Geological Survey of Namibia, Geological Survey of Namibia Series,* vol. 12, edited by R. Miller, pp. 89–98, Geological Survey of Namibia, Windhoek.

Mareschal, M., R. L. Kellett, R. D. Kurtz, J. N. Ludden, S. Ji, and R. C. Bailey (1995), Archaean cratonic roots, mantle shear zones and deep electrical anisotropy, *Nature*, *375*(6527), 134–137, doi:10.1038/375134a0.

Martí, a., P. Queralt, J. Ledo, and C. Farquharson (2010), Dimensionality imprint of electrical anisotropy in magnetotelluric responses, *Phys. Earth Planet. Inter.*, *182*, 139–151, doi:10.1016/j.pepi.2010.07.007.

Martin, H., and H. Porada (1977), The intra-cratonic branch of the Damara orogen in South West Africa I: Discussion of geoddynamic models, *Precambrian Res.*, *5*, 311–338.

McDermott, F., N. B. W. Harris, and C. J. Hawkesworth (2000), Geochemical constraints on the petrogenesis of Pan-African A-type granites in the Damara Belt, Namibia, in *Henno Martin Commemorative Volume: Communications of the Geological Survey of Namibia, Special Publication of the Geol. Survey of Namibia,* vol. 12, edited by R. M. G. Miller, pp. 139–148, Geol. Soc. Survey of Namibia, Windhoek.

McNeice, G. W., and A. G. Jones (2001), Multisite, multifrequency tensor decomposition of magnetotelluric data, *Geophysics*, *66*, 158–173.

Miensopust, M. P., and A. G. Jones (2011), Artefacts of isotropic inversion applied to magnetotelluric data from an anisotropic Earth, *Geophys. J. Int.*, *187*, 677–689, doi:10.1111/j.1365-246X.2011.05157.x.

Miensopust, M. P., A. G. Jones, M. Muller, X. Garcia, and R. L. Evans (2011), Lithospheric structures and precambrian terrane boundaries in northeastern Botswana revealed through magnetotelluric profiling as part of the southern African magnetotelluric experiment, *J. Geophys. Res.*, *116*, B02401, doi:10.1029/2010JB007740.

Miller, R. M. G. (1983), The Pan African Damara Orogen of Namibia, in *Evolution of the Damara Orogen of Southwest Africa/Namibia, Special Publication of the Geol. Soc. South Africa,* vol. 11, edited by R. M. G. Miller, pp. 431–515, Geol. Soc. South Africa, South Africa.

Miller, R. M. G. (ed.) (1988), *Geological Map of the Damara Orogen, Namibia (scale 1:500,000)*, pp. 1–2, Geological Survey of Namibia, Windhoek, Namibia.

Modisi, M. P., E. A. Atekwana, A. B. Kampunzu, and T. H. Ngwisanyi (2000), Rift kinematics during the incipient stages of continental extension: Evidence from the nascent Okavango rift basin, Northwest Botswana, October(July 2009), *Geology*, *28*(10), 939–942, doi:10.1130/0091-7613(2000)28<939.

Muller, M. R., A. G. Jones, R. L. Evans, S. Evans, C. J. S. Fourie, X. Garcia, A. Mountford, J. E. Spratt, and S. M. Team (2009), Lithospheric structure, evolution and diamond prospectivity of the Rehoboth Terrane and Western Kaapvaal Craton, Southern Africa: Constraints from broadband magnetotellurics, *Lithos*, *112*, 93–105, doi:10.1016/j.lithos.2009.06.023.

Niblett, E. R., and C. Sayn-Wittgenstein (1960), Variation of electrical conductivity with depth by the magneto-telluric method, *Geophysics*, *25*, 998–1008.

O'Neill, C., L. Moresi, and a. Jaques (2005), Geodynamic controls on diamond deposits: Implications for Australian occurrences, *Tectonophysics*, *404*(3-4), 217–236, doi:10.1016/j.tecto.2005.04.010.

Parker, R. L., and J. R. Booker (1996), Optimal one-dimensional inversion and bounding of magnetotelluric apparent resistivity and phase measurements, *Phys. Earth Planet. Inter.*, *98*(3-4), 269–282, doi:10.1016/S0031-9201(96)03191-3.

Peslier, A. H., A. B. Woodland, D. R. Bell, and M. Lazarov (2010), Olivine water contents in the continental lithosphere and the longevity of cratons, *Nature*, *467*, 78–81, doi:10.1038/nature09317.

Porada, H. (1989), Pan-African rifting and orogenesis in southern to equatorial Africa and Eastern Brazil, *Precambrian Res.*, *44*(2), 103–136, doi:10.1016/0301-9268(89)90078-8.

Prave, A. R. (1996), Tale of three cratons: Tectonostratigraphic anatomy of the Damara orogen in northwestern Namibia and the assembly of Gondwana, *Geology*, *24*(12), 1115–1118, doi:10.1130/0091-7613(1996).

Raab, M. (2002), Late Cretaceous reactivation of major crustal shear zones in northern Namibia: Constraints from apatite fission track analysis, *Tectonophysics*, *349*(1-4), 75–92, doi:10.1016/S0040-1951(02)00047-1.

Reeves, C. V. (1972), Rifting in the Kalahari? *Nature*, *237*(5350), 95–96, doi:10.1038/237095a0.

Ritter, O., U. Weckmann, T. Vietor, and V. Haak (2003), A magnetotelluric study of the Damara belt in Namibia 1. Regional scale conductivity anomalies, *Phys. Earth. Planet. Int.*, *138*, 71–90, doi:10.1016/S0031-9201(03)00078-5.

Rodi, W., and R. L. Mackie (2001), Nonlinear conjugate gradients algorithm for 2D magnetotelluric inversion, *Geophysics*, *66*, 174–187.

Sasaki, Y., and M. A. Meju (2006), Three-dimensional joint inversion for magnetotelluric resistivity and static shift distributions in complex media, *J. Geophys. Res.*, *111*, B05101, doi:10.1029/2005JB004009.

Selway, K., G. Heinson, and M. Hand (2006), Electrical evidence of continental accretion: Steeply-dipping crustal-scale conductivity contrast, *Geophys. Res. Lett.*, *33*, L06305, doi:10.1029/2005GL025328.

Selway, K., S. Sheppard, A. Thorne, S. Johnson, and P. Groenewald (2009), Identifying the lithospheric structure of a precambrian orogen using magnetotellurics: The Capricorn Orogen, Western Australia, *Precambrian Res.*, *168*, 185–196.

Singletary, S. J., R. E. Hanson, M. W. Martin, J. L. Crowley, S. A. Bowring, R. M. Key, L. V. Ramokate, B. B. Direng, and M. A. Krol (2003), Geochronology of basement rocks in the Kalahari Desert, Botswana, and implications for regional Proterozoic tectonics, *Precambrian Res.*, *121*(25), 47–71, doi:10.1016/S0301-9268(02)00201-2.

Siripunvaraporn, W., and G. Egbert (2000), An efficient data-subspace inversion method for 2-D magnetotelluric data, *Geophysics*, *65*, 791–803.

Siripunvaraporn, W., and G. Egbert (2009), WSINV3DMT: Vertical magnetic field transfer function inversion and parallel implementation, *Phys. Earth Planet. Inter.*, *173*, 317–329.

Siripunvaraporn, W., G. Egbert, Y. Lenbury, and M. Uyeshima (2005), Three-dimensional magnetotelluric inversion: Data-space method, *Phys. Earth Planet. Inter.*, *150*, 3–14, doi:10.1016/j.pepi.2004.08.023.

Smith, J., and J. Booker (1991), Rapid inversion of two- and three-dimensional magnetotelluric data, *J. Geophys. Res.*, *96*, 3905–3922.

Spratt, J. E., A. G. Jones, V. A. Jackson, L. Collins, and A. Avdeeva (2009), Lithospheric geometry of the Wopmay orogen from slave craton to bear province magnetotelluric transect, *J. Geophys. Res.*, *114*, B01101, doi:10.1029/2007JB005326.

Trompette, R. (1997), Neoproterozoic (600 Ma) aggregation of Western Gondwana: A tentative scenario, *Precambrian Res.*, *82*(1-2), 101–112, doi:10.1016/S0301-9268(96)00045-9.

Unsworth, M., W. Wenbo, A. G. Jones, S. Li, P. Bedrosian, J. Booker, J. Sheng, D. Ming, and T. Handong (2004), Crustal and upper mantle structure of Northern Tibet imaged with magnetotelluric data, *J. Geophys. Res.*, *109*, B02403, doi:10.1029/2002JB002305.

van Zijl, J. S. V., and J. H. de Beer (1983), Electrical structure of the Damara orogen and its tectonic significance, *Spec. Publ. Geol. Soc. S. Afr.*, *11*, 369–379.

Walter, J. M. (2004), Fabric development, electrical conductivity and graphite formation in graphite-bearing marbles from the central Damara, Ph.D. thesis, University of Göttingen.

Wannamaker, P. (2005), Anisotropy versus heterogeneity in continental solid earth electromagnetic studies: Fundamental response characteristics and implications for physicochemical state, *Surv. Geophys.*, *26*, 733–765.

Weckmann, U. (2003), A magnetotelluric study of the Damara Belt in Namibia 2. MT phases over 90 reveal the internal structure of the Waterberg Fault/Omaruru Lineament, *Phys. Earth Planet. Inter.*, *138*(2), 91–112.

Wessel, P., and W. H. F. Smith (1991), Free software help map and display data, *EOS Trans. AGU*, *72*, 441–446.

Wessel, P., and W. H. F. Smith (1998), New, improved version of the generic mapping tools released, *EOS Trans. AGU*, *79*(47), 579–579.

Whitehead, K., A. le Roex, C. Class, and D. Bell (2002), Composition and cretaceous thermal structure of the upper mantle beneath the damara mobile belt: Evidence from nephelinite-hosted peridotite xenoliths, swakopmund, namibia, *J. Geol. Soc. London*, *159*, 307–321, doi:10.1144/0016-764901-113.

Wu, X., I. J. Ferguson, and A. G. Jones (2005), Geoelectric structure of the Proterozoic Wopmay Orogen and adjacent terranes, Northwest Territories, *Earth*, *981*, 955–981, doi:10.1139/E05-042.

Xu, Y. (2000), Pressure effect on electrical conductivity of mantle olivine, *Phys. Earth Planet. Inter.*, *118*(1-2), 149–161, doi:10.1016/S0031-9201(99)00135-1.

Yoshino, T., T. Matsuzaki, S. Yamashita, and T. Katsura (2006), Hydrous olivine unable to account for conductivity anomaly at the top of the asthenosphere, *Nature*, *443*, 973–976.

Zhdanov, M. S., S. K. Lee, and K. Yoshioka (2006), Integral equation method for 3D modeling of electromagnetic fields in complex structures with inhomogeneous background conductivity, *Geophysics*, *71*, G333–G345.